

MICROCOPY RESOLUTION TEST CHART
NATIONAL BUREAU OF STANDARDS-1963-A

(Handwritten mark)

AFGL-TR-84-0261

POLAR MOTIONS MEASUREMENT STUDY

Joel Hanse
Werner H. Egli
Mario Ignagni

Honeywell Systems and Research Center
2600 Ridgway Parkway, PO Box 312
Minneapolis, Minnesota 55440

Final Report
May 1983 - July 1984

September 1984

Approved for public release; distribution unlimited

DTIC FILE COPY

AIR FORCE GEOPHYSICS LABORATORY
AIR FORCE SYSTEMS COMMAND
UNITED STATES AIR FORCE
HANSKOM AFB, MASSACHUSETTS 01731

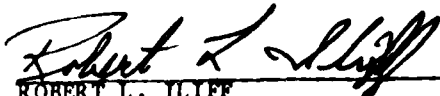
DTIC
ELECTE
MAR 1 1985
S D
A

85 02 15 104

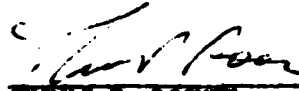
AD-A150690

CONTRACTOR REPORTS

This technical report has been reviewed and is approved for publication.



ROBERT L. ILIFF
Contract Manager



THOMAS P. ROONEY
Chief, Geodesy & Gravity Branch

FOR THE COMMANDER



DONALD H. ECKHARDT
Director
Earth Sciences Division

This report has been reviewed by the ESD Public Affairs Office (PA) and is releasable to the National Technical Information Service (NTIS).

Qualified requesters may obtain additional copies from the Defense Technical Information Center. All others should apply to the National Technical Information Service.

If your address has changed, or if you wish to be removed from the mailing list, or if the addressee is no longer employed by your organization, please notify AFGL/DAA, Hanscom AFB, MA 01731. This will assist us in maintaining a current mailing list.

REPORT DOCUMENTATION PAGE		READ INSTRUCTIONS BEFORE COMPLETING FORM
1. REPORT NUMBER AFGL-TR-84-0261	2. GOV'T ACCESSION NUMBER A150 690	3. RECIPIENT'S CATALOG NUMBER
4. TITLE (AND SUBTITLE) Polar Motions Measurement Study		5. TYPE OF REPORT/PERIOD COVERED Final Report May 1983 to July 1984
7. AUTHOR(S) Dr. Joel Hanse, Werner H. Egli, and Mario Ignagni		6. PERFORMING ORG. REPORT NUMBER 84SRC41
9. PERFORMING ORGANIZATIONS NAME/ADDRESS Honeywell Systems and Research Center 2600 Ridgway Parkway, PO Box 312 Minneapolis, Minnesota 55440		8. CONTRACT OR GRANT NUMBER(S) Contract No. F19628-83-C-0103
11. CONTROLLING OFFICE NAME/ADDRESS Air Force Geophysics Laboratory Hanscom AFB, Massachusetts 01731 Monitor/ Robert Iliff/LWC		10. PROGRAM ELEMENT PROJECT, TASK AREA & WORK UNIT NUMBERS 62101F 3201DMAH
14. MONITORING AGENCY NAME/ADDRESS (IF DIFFERENT FROM CONT. OFF.)		12. REPORT DATE September 1984
		13. NUMBER OF PAGES 119
		15. SECURITY CLASSIFICATION (OF THIS REPORT) Unclassified
		15a. DECLASSIFICATION DOWNGRADING SCHEDULE
16. DISTRIBUTION STATEMENT (OF THIS REPORT) Approved for public release; distribution unlimited		
17. DISTRIBUTION STATEMENT (OF THE ABSTRACT ENTERED IN BLOCK 20, IF DIFFERENT FROM REPORT)		
18. SUPPLEMENTARY NOTES		
19. KEY WORDS (CONTINUE ON REVERSE SIDE IF NECESSARY AND IDENTIFY BY BLOCK NUMBER) crustal motion, subarc-second, laser gyro, earth spin axis deviation, measurement, ring laser gyro, northfinder, polar axis deviation,		
20. ABSTRACT (CONTINUE ON REVERSE SIDE IF NECESSARY AND IDENTIFY BY BLOCK NUMBER) In this report we analyze the feasibility of subarc-second measurement of earth crust warp and/or earth spin axis deviation, in less than one day, using ring laser gyroscopes and accelerometers and/or tiltmeters. It is marginally feasible, using laser gyros equivalent to the Honeywell GG1389, either unidirectionally carouseled or with enhancement equivalent to Honeywell closed-loop lockin correction (CLIC). Experimental results on the GG1389 show that input axis stability is more than adequate, and that its carouseled or CLIC-enhanced random drift and output resolution suffice marginally. - cont (continued)		

20. (continued)

Design and build of a one-axis feasibility demonstrator is recommended, using one CLIC-enhanced GG1389 ring laser gyro, two state-of-the-art tiltmeters, an Ultradex indexer, and a Hewlett-Packard micro-computer. *→ not necessary include*

see 177

FOREWORD

This report describes the Polar Motions Measurement Study applied research task done by Honeywell Systems and Research Center for the Air Force Geophysics Laboratory, under Contract No. F19628-83-C-0103.

Publication of this report does not constitute approval by the Air Force Geophysics Laboratory of the findings and/or conclusions contained herein. This report is published solely to stimulate the free exchange of ideas and information.



CONTENTS

Section		Page
1	INTRODUCTION AND SUMMARY	1
2	PRELIMINARY STUDIES	4
	Assumptions	4
	Configurations and Principles of Operation	5
	Basic Analysis of System Operation	6
	Resolution of Distinguishability	10
	Dual-Freedom Strapdown Concept	13
	Dual-Freedom Strapdown Rotational Strategy	15
3	SENSOR AND SYSTEM ERROR MODELS	17
	Gyro Rate White Noise	17
	Sensor Quantization	18
	Parameter Variation	19
	Compliance-Related Errors	23
4	SYSTEM ERROR STUDIES	27
	Error Propagation in Dual-Freedom System	27
	Covariance Analysis and Kalman Estimation	30
	Formulation of Dual-Freedom System Simulation	34
	Results of Dual-Freedom System Simulation	38
	Discussion of Simulation Results	41
5	ONE-AXIS SYSTEM STUDY	45
	Error Analysis	45
	Gyro Performance Requirements	48

CONTENTS (concluded)

Section		Page
	Expected System Performance	50
	Hardware Requirements	51
	Gyro Modifications Needed	52
6	EXPERIMENTAL RESULTS	56
	Undithered Gyro Random Drift Characteristics	56
	Input Axis Stability Tests	57
	Tiltmeter Characteristics	70
7	CONCLUSIONS AND RECOMMENDATIONS	73
	Conclusions	73
	Recommendations	74
	Recommended Demonstrator Design	74
	Demonstrator Features	77
APPENDIX A	ANALYSIS OF DUAL-FREEDOM ROTATIONAL STRATEGY	79
APPENDIX B	NAVIGATION ERROR MODEL	93
APPENDIX C	SENSOR QUANTIZATION ERROR MODEL	103

LIST OF ILLUSTRATIONS

Figure		Page
1	Evolution of Dual-Freedom Strapdown Triad	14
2	Dual-Freedom Sensor Assembly Rotational Profile	16
3	Sample Time Histories of Three Stochastic Processes	21
4	Attitude Error Propagation in a Rotational System	28
5	Simulated North-South rms Error, Using GG1300s	39
6	Simulated Vertical rms Error, Using GG1300s	40
7	Simulated East-West rms Error, Using GG1389s	41
8	Simulated North-South rms Error, Using GG1389s	42
9	Simulated Vertical rms Error, Using GG1389s	42
10	GG1389 Random Drift Analysis, 17 January 1984	57
11	GG1389 Random Drift Analysis, 19 January 1984	57
12	GG1389 Random Drift Analysis, 20 January 1984	58
13	Input Axis Stability Test Setup, Side View	60
14	Input Axis Stability Test Setup, Front View	60
15	Stability of Bubble Tiltmeter (over 12 months)	71
16	Block Diagram of Proposed Demonstrator Hardware	75
17	Block Schematic of Demonstrator Electronics	76

LIST OF TABLES

Table		Page
1	1 σ Errors Assumed for Three-Axis Simulation	37
2	Short-Term Axis Stabilities of GG1389 No. 011	66
3	Multiday Data of GG1389 No. 011	66
4	Multiday Stabilities of GG1389 No. 011	67
5	Multi-Orientation Data for GG1389 No. 009	67
6	Short-Term Axis Stabilities of GG1389 No. 009	68
7	Multiday Data of GG1389 No. 009	68
8	Multi-Orientation Data for GG1389 No. 004	69
9	Multiday Data of GG1389 No. 004	69
10	Short-Term Axis Stabilities of GG1389 No. 004	70
11	Multiday Stabilities of GG1389 No. 004	70

SECTION 1

INTRODUCTION AND SUMMARY

This 15-month applied research program was aimed at determining the feasibility of making subarc-second quality measurements of earth crustal deviation and earth polar axis wander using ring laser gyro (RLG) based systems.

The program comprised analyses of the performance of two selected system configurations and rate table laser gyro testing. This final report describes the work done and the results obtained, presents conclusions on the feasibility of making subarc-second measurements of earth polar axis (EPA)/crustal deviations, and frames recommendations for further work.

The two configurations selected consisted of a three-axis navigator system, using three laser gyros, three accelerometers, and compound gimbaling; and a one-axis system, comprising one laser gyro, two tiltmeters, and indexation to point the gyro alternately east and west.

The laser gyro selected for both the analyses and the testing phases of this program was the Honeywell GG1389 gyro. This state-of-the-art gyro is probably the finest in the world.

Preliminary analysis showed that it is impossible to distinguish earth crustal deviation around the vertical from EPA wander along the east-west axis, using self-contained inertial measurements.

Preliminary calculations based on GG1389 gyros with computer-driven random drift reduction showed that, in a kinematically benign environment, combined crustal deviation and polar axis east-west wander could be determined with subarc-second accuracy over less than 24 hr.

Based on these preliminary results, we defined a reasonable performance goal: determine the 16-hr average value of combined earth crustal deviation and EPA deviation, within 0.2 arc-sec rms, over a 16-hr period, in a benign environment.

Using covariance analysis as needed, a linear error propagation model, and known and extrapolated component characteristics, our analyses showed that the simple one-axis system should perform as well as the three-axis navigator system, and that both could come close to reaching the performance goal. Rate table tests on Honeywell GG1389 RLGs showed that this gyro's performance is now almost compatible with the performance goal. The crucial characteristics are random drift and input axis stability.

The random drift was about $0.000045^\circ/\text{rt-hr}$, when operated in the scale-factor mode (i.e., continuously rotated without dithering). The input axis stability ranged from 0.004 to 0.04 arc-sec, relative to the gyro body structure, and from 0.25 to 0.90 arc-sec across removals and remountings of the gyros.

The low random drift performance could be retained when operating in the dithered mode by using a real-time computer-controlled laser gyro random drift improvement technique, called CLIC, invented by Honeywell. Although still not operative under general input rate environments, CLIC will reliably improve dithered laser gyro random drift under benign environments, down to near quantum limited performance.

It is reasonable to suppose that careful design of an indexed system should improve the input axis stability, from the above 0.25 to 0.90 arc-sec mount/remount value, down towards the 0.04 arc-sec intrinsic value. This could be achieved by improving the quality of the mounting geometry, and/or by directly measuring the mounting misalignment and compensating the system output.

The tiltmeters used in the one-axis system would contribute negligible added error to that from gyro random drift. Tiltmeters are readily manufactured with subarc-second resolution and multi-hour stability. In the three-axis navigator, the accelerometers would make a larger error contribution (it is more difficult to make ultrasensitive and ultrastable accels than tiltmeters), but still minor compared to that from the gyros.

Considering the foregoing results and arguments, we conclude that it is feasible to make subarc-second measurements of combined EPA deviation and earth crustal rotational displacements, over less than one day, using a RLG-based system, in a configuration as simple as the one-gyro-plus-two-tiltmeter device.

We recommend that the Air Force Geophysics Laboratory (AFGL) design and build a one-axis demonstrator unit, as described herein, to be tested by AFGL under field conditions, as a prelude to designing and building a more elaborate unit with all features needed to function as an autonomous transportable field model sensor.

SECTION 2

PRELIMINARY STUDIES

ASSUMPTIONS

We defined the set of assumptions under which the study would proceed, as listed below.

- o Rigid-earth geography: invariant distances between all surface features recognized as fixed in the everyday sense. Terrains such as glaciers, icefloes, etc., excluded. Intercontinental drifts considered negligible.
- o Despite the rigidity as defined above, local short-range twist deformations occur. These are to be determined to within subarc-second accuracy, over less than one day.
- o Gravity vector at any location is constant, expressed in a geographic reference frame affixed to the rigid earth.
- o Earth polar spin axis will deviate from nominal orientation, as seen in rigid-earth reference frame. This deviation is to be determined with subarc-second accuracy over less than a day. Polar axis wander during the measurement period is negligible.
- o Crustal twist and polar axis deviation to be determined using a substantially self-contained device (e.g., without need for star shots, triangulation, etc.).
- o Benign environment: fixed position, zero velocity, and zero kinematic acceleration, all specific force is gravitational.

CONFIGURATIONS AND PRINCIPLES OF OPERATION

We selected two system configurations for study. One of these was a high-precision three-axis inertial navigator, with three RLGs and three accelerometers. The other was a stripped system, designed to exploit the advantages of operation under ultra-benign kinematic environment. It consists of a single gyro, whose input axis lies along nominal east-west, and two tiltmeters, which measure tilt around the north-south and the east-west axes, with 180° indexing around nominal vertical, to enable bias cancellation. The principle behind both systems is to define earth crustal twist and EPA deviation in terms of a reference frame defined by the local vertical and the nominal EPA.

The accels (or tiltmeters) define the local vertical (unit g-vector) as seen in the body frame of the device. The angle sensor(s) define the total rotation vector (earth spin + body rate), also as seen in the body frame. North is defined as lying along the horizontal component of earth spin, which is nominally of value $E \cdot \cos(LT)$, where E is full earth rate (about 15°/hr), and LT is latitude.

Body tilt around the north-south axis through an angle $A(NS)$ will add a spin component along east-west of value $E \cdot \sin(LT) \cdot A(NS)$, comprising the rotated vertical component of earth spin. This will deflect the total spin vector east-westwards through an angle of $(E \cdot \sin(LT) \cdot A(NS)) / (E \cdot \cos(LT))$, = $A(NS) \cdot \tan(LT)$. This is, of course, easily corrected for by using the north-south tilt angle, $A(NS)$, which is arrived at by interpreting the accel/tiltmeter readings.

Body rate around the east-west axis of value $R(EW)$ will sum vectorially with the earth spin vector to produce a total spin vector whose horizontal component is deviated east/westwards from north, through an angle of $R(EW) / (E \cdot \cos(LT))$.

It will also rotate the sensed local vertical at rate $R(EW)$ around east-west. This can be seen in the rate of change of the accel signals, and thus east-west tilt rate can also be corrected for.

However, deviation in the horizontal component of earth rate cannot be detected when using only the g -vector in addition to earth rate. The effect of, say, a 1 arc-sec rotation of the horizontal part of earth rate, from true north to north + 1 arc-sec east, cannot be distinguished from the effect of a rotation of the body on which the gyro is mounted, through an angle of 1 arc-sec counterclockwise around the vertical.

This is the distinguishability problem: how does one determine EPA deviation, while using the EPA as one "leg" of the reference frame in which the deviation is to be expressed? (The other "leg" is the local vertical.) Obviously, the only detectable kind of EPA deviation would be that causing a change in the angle between the EPA and vertical, i.e., meridional deviation. East-west deviation would be undetectable.

BASIC ANALYSIS OF SYSTEM OPERATION

Let the earth spin rate vector, including deviation, be denoted:

$$e = E + d,$$

where:

e = deviated earth spin rate vector

E = nominal earth spin rate vector

d = deviation vector, whose direction denotes the axis, and whose magnitude denotes the amount of the spin rate deviation

Let the crustal warp be denoted by a small rotation vector, a , whose direction represents the axis, and whose magnitude represents the angle of warp. Let the

crustal warp rate be denoted as the rotation rate vector, p , whose direction represents the axis, and whose magnitude denotes the amount of the warp rate.

Rigid-earth coordinates are defined in terms of unit vectors i along east, j along north, and k along the upward-vertical. The nominal earth-spin, E , is expressed as

$$E = R(j \cdot \cos(L) + k \cdot \sin(L))$$

where:

R = nominal spin rate (about $15.04107^\circ/\text{hr}$)

L = nominal latitude

Similarly, we denote the warp angle vector, a , as

$$a = i \cdot a_1 + j \cdot a_2 + k \cdot a_3$$

the warp rate vector, p , as

$$p = i \cdot p_1 + j \cdot p_2 + k \cdot p_3$$

and the earth spin rate deviation, d , as

$$d = i \cdot d_1 + j \cdot d_2 + k \cdot d_3$$

Further assume that the environment is so benign that, averaged over the period of observation, all that the accels sense are components of the gravity vector, seen along the sensing axes of the accels. Then, we can substitute tiltmeters for the accels. The tiltmeters will simply (and sufficiently) indicate the direction only (no magnitude) of the gravity vector, and they will do so more accurately than accels would. Now suppose that the following quantities are

determined over the period of measurement, as perceived in the crustally warped body axes:

Average net sensed rotation rate, e

Average sensed unit gravity vector, g

Average rate of change of sensed gravity vector, g'

By simple kinematics, putting the true value of the gravity vector equal to k :

$$e = E + d + p + a \times E,$$

$$g = k + a \times k$$

$$g' = p \times k$$

where \times denotes the vector cross-product operator.

Substituting the vectorial component representations for E , d , p , and a , we get:

$$\begin{aligned} e = & i*(R*(a2*\sin(L) - a3*\cos(L)) + d1 + p1) \\ & + j*(d2 + p2 - R*a1*\sin(L)) \\ & + k*(d3 + p3 + R*a1*\cos(L)) \end{aligned}$$

$$g = i*a2 - j*a1 + k$$

$$g' = i*p2 - j*p1$$

The components seen along the three axes i , j , and k are, for the rate sensing observation:

$$e1 = R*(a2*\sin(L) - a3*\cos(L)) + d1 + p1$$

$$e2 = d2 + p2 - R*a1*\sin(L)$$

$$e3 = d3 + p3 + R*a1*\cos(L)$$

for the tilt observations:

$$g_1 = a_2$$

$$g_2 = -a_1$$

$$g_3 = 1$$

and for the tilt-rate observations:

$$g'_1 = p_2$$

$$g'_2 = -p_1$$

$$g'_3 = \text{zero}$$

From these, we get the partial set of solutions:

$$a_1 = -g_2$$

$$a_2 = g_1$$

$$p_1 = -g'_2$$

$$p_2 = g'_1$$

Substituting in the rate-sensing observations, we get:

$$d_1 - R \cdot a_3 \cdot \cos(L) = e_1 - R \cdot g_1 \cdot \sin(L) + g'_2$$

$$d_2 = e_2 - R \cdot g_2 \cdot \sin(L) - g'_1$$

$$d_3 + p_3 = e_3 + R \cdot g_2 \cdot \cos(L)$$

This shows that we can determine a_1 , a_2 , p_1 , p_2 , and d_2 , but that we can only determine d_3 and p_3 in the combination $d_3 + p_3$, and d_1 and a_3 in the combination $d_1 - R \cdot a_3 \cdot \cos(L)$. In some situations, we may know a priori that the vertical axis component, p_3 , of the warp rate vector, p , is zero. Then, d_3 can also be determined, but there remains the indistinguishability between the east-west component of earth spin vector wander, d_1 , and the vertical axis component of

crustal warp rotation, a_3 . Hence, inertial measurements don't suffice to define the deviation of the earth spin vector, nor the local crustal rotational warp. Therefore, we cannot use inertial measurements alone to orient to the earth-fixed reference frame.

RESOLUTION OF DISTINGUISHABILITY

Within the constraint of avoiding the use of astronomical scale fixes, such as lunar laser ranging, star shots, etc., there are three ways of dealing with this problem. One of these is to use a high-quality theodolite, affixed to the device to be oriented, and landmark(s) at a sufficient distance from the viewing point, in the horizon plane. A sufficient distance means far enough away so that effects of landmark crustal rotation are attenuated to zero (but not so far as to give excessive refraction errors). How far remains to be determined, as a function of what's needed and what's possible. Clearly, the wall of a small chamber housing the apparatus would be a poor landmark; distances of several hundred meters would probably be needed. This would enable determination of crustal rotation and rotation rate around the vertical axis (a_3 and p_3 , respectively), to the accuracy of the theodolite-operator system.

The average rotation angle around the vertical would be the average of some number of equi-time-spaced readings of azimuthal deviation, taken over the observation period. The average rotation rate around the vertical would, in principal, be the difference between an initial azimuthal deviation reading and a final one, divided by the time difference between the two readings. In practice, this may be refined by best-fitting to all the azimuthal deviation readings. The accuracy of individual theodolite fixes is about 1 arc-sec, rms. If this is random independent "white noise" error, 100 successive fixes would average the error down to 0.1 arc-sec rms. Very likely, one would have to take successive fixes incessantly. Well-correlated fix error could be a major problem.

The expected plethora of theodolite fixes would, of course, be passed into a computer. However, this method could still be very labor-intensive, because of the multitude of readings to be taken, and because of the indexing, plunging, and what-have-you that accompanies theodolite readings, in order to cancel some of the systematic errors. Some of this could doubtless be automated, but there would still be demands on the operator. For these reasons, and because of the eventual environment the system might be required to operate in, this approach was dropped from further consideration.

The second method of dealing with the distinguishability problem is to use independently determined earth spin vector values. Then, we know the values of d_1 , d_2 , and d_3 , and we get a_3 and p_3 by:

$$a_3 = (d_1 - e_1 + R*g_1*\sin(L) - g'^2)/(R*\cos(L))$$

$$p_3 = e_3 + R*g_2*\cos(L) - d_3$$

The earth spin vector is a world constant. So, it can be determined at any convenient location and its value then transmitted to a multitude of sites. The value is then easily transformed into a local coordinate system expression. Specifically, let the deviation be expressed as the vectorial sum of a polar deviation (i.e., a deviation in magnitude), DM , a deviation along the Greenwich meridian, DG , and a deviation along the 90° east meridian, DE . Then, at latitude LN north and longitude LE east, the locally-seen earth spin deviation vector is

$$d = i*(DG*\sin(LE) + DE*\cos(LE))$$

$$+ j*(DM*\cos(LN) + \sin(LN)*(DG*\cos(LE) - DE*\sin(LE)))$$

$$+ k*(DM*\sin(LN) - \cos(LN)*(DG*\cos(LE) - DE*\sin(LE)))$$

i.e.,

$$d1 = DG*\sin(LE) + DE*\cos(LE)$$

$$d2 = DM*\cos(LN) + \sin(LN)*(DG*\cos(LE) - DE*\sin(LE))$$

$$d3 = DM*\sin(LN) - \cos(LN)*(DG*\cos(LE) - DE*\sin(LE))$$

In principle, measuring the exact earth spin vector at a central location is no easier than doing it at a multitude of sites. But, it may be possible to find locations where the earth crustal warp is essentially zero, e.g., on some special underground bedrock granite formation, far removed from seismic epicenters. These determinations could be intermittently checked by star sightings, whenever the "seeing" is favorable. The assumption is that some special earth-spin-measurement laboratory can be set up at some favorable location(s) to provide continuous values good to within 0.1 arc-sec rms.

There is a third possibility, suggested by our perception of the ultimate application by the customer (AFGL). It appears that the system could eventually be deployed at a large number of sites, N, with measurements taken fairly frequently. Furthermore, it would be reasonable to assume that the crustal warps at all N sites would constitute a zero-mean random independent set. Consequently, the multi-site mean crustal rotation around vertical should be zero, with an rms deviation around that value of magnitude $1/\text{SQRT}(N)$ times the rms value of individual site crustal rotations around the multi-site mean. If so, the individual determinations of site crustal rotation plus earth axis deviation should, upon multi-site averaging, produce an estimate of earth axis deviation, corrupted by $1/\text{SQRT}(N)$ times the rms crustal deviation. Actually, the computation would be somewhat more complex than the above, especially if the sites were well separated on the earth surface. In that case, the averaging would have to include the fact that earth spin axis deviation will be seen differently at each of the N locations. It would, in fact, be a straightforward least-squares best-fit procedure.

DUAL-FREEDOM STRAPDOWN CONCEPT

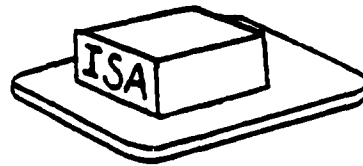
Northfinding/leveling is performed routinely by all inertial navigation systems as a preliminary to entering the navigation phase. Accuracy of northfinding is typically about 1 mrad, achieved in 15 min. The major factors affecting accuracy are gyro biases (fixed and random) and accelerometer biases.

In order to enhance performance, we may rotate the inertial sensor assembly (ISA) about one or more axes, called carouseling. By so doing, the effect of gyro and accelerometer fixed biases may be partially or totally eliminated, depending on the number of axes of carouseling.

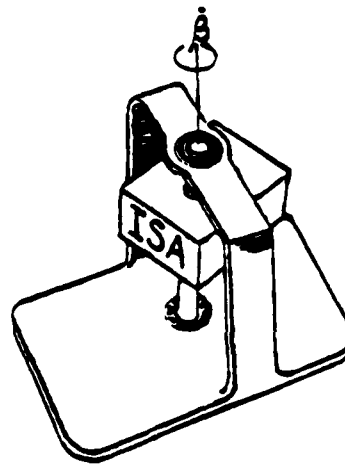
In a pure strapdown system (see Figure 1a), attitude error is essentially the time integral of all gyro error terms. In order to reduce the error, the inertial sensors may be mounted to a rotating base, rather than to a fixed one (see Figure 1b). Partial commutation or averaging of systematic gyro errors results. There is a reduced attitude error for axes in the plane of rotation, but none for the the out-of-plane one. (It does not help to dispose the three gyros so that all three gyro axes partake of the rotation.)

Further attenuation is provided by a dual-freedom strapdown approach, in which the plane of the rotating turntable is itself being rotated (see Figure 1c). If both rotational axes are properly controlled, it is possible to get almost bounded attitude errors over very long time periods, due to constant gyro errors such as bias, scale factor error, and misalignment. There is, however, no reduction of the error due to dithered laser gyro random walk.

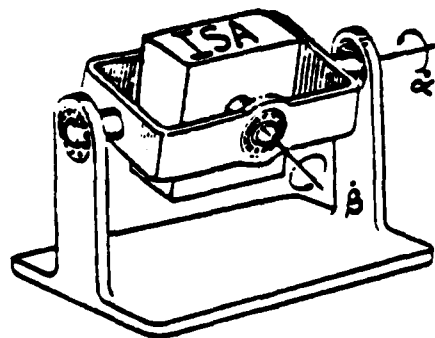
Having thus dealt with systematic error sources, the final step is to rate-bias the gyros to eliminate random walk. The three gyros are maintained in uninterrupted unidirectional rotation, rather than being dithered in periodic motion. This eliminates the lock-in error increments that occur as the gyro rotation rate goes through zero twice per dither cycle, and hence eliminates



a. Pure strapdown



b. Single-freedom strapdown



c. Dual-freedom strapdown

Figure 1. Evolution of Dual-Freedom Strapdown Triad

the resultant random walk. To do this on the dual-freedom approach, we elevate the gyro input axes above the equatorial plane, so that all three gyros receive a portion of the angular rate about the inner axis, and we slip-ring the inner axis, to allow continuous rotation.

To summarize, pure strapdown is the simplest approach, but has the greatest attitude error growth. The single- and dual-freedom approaches attenuate, respectively, some and all of the attitude error due to fixed gyro errors, without any reduction of that part due to random walk. Finally, dual-freedom strapdown with rate-biasing eliminates virtually all errors. This is the configuration that we have selected for analysis and simulation.

DUAL-FREEDOM STRAPDOWN ROTATIONAL STRATEGY

Appendix A shows that two conditions suffice to enable successful dual-freedom strapdown rotational strategy

1. The inner axis rate is an integer multiple of the outer axis rate.
2. The outer axis reverses direction at 360° traverse intervals.

These ensure the commutation of gyro and accelerometer bias, scale factor, and misalignment errors.

The Appendix A analysis assumed that the outer axis can reverse direction instantaneously, and that there are no nonlinearity errors in the sensor outputs. But, the analysis can be extended by expressing all quantities appearing in Appendix A tables as Fourier series over one cycle of the outer axis. This leads to a refined dual-axis rotational profile that gives periodic cancellation of the following sensor errors.

- * gyro bias errors
- * gyro linear scale factor errors
- * gyro misalignment errors
- * gyro scale factor asymmetry and nonlinearity errors
- * accelerometer bias errors
- * accelerometer linear scale factor errors
- * some accelerometer scale-factor nonlinearity errors (all odd powers, 0th and 2nd even powers only)
- * accelerometer misalignment errors

An example of error-cancelling gimbal angle profiles is shown in Figure 2. The outer gimbal rates consist of zero rate segments, constant rate segments, and ramp rate segments. More generally, error cancellation is provided when each segment of the outer axis rate profile is symmetric about its midpoint.

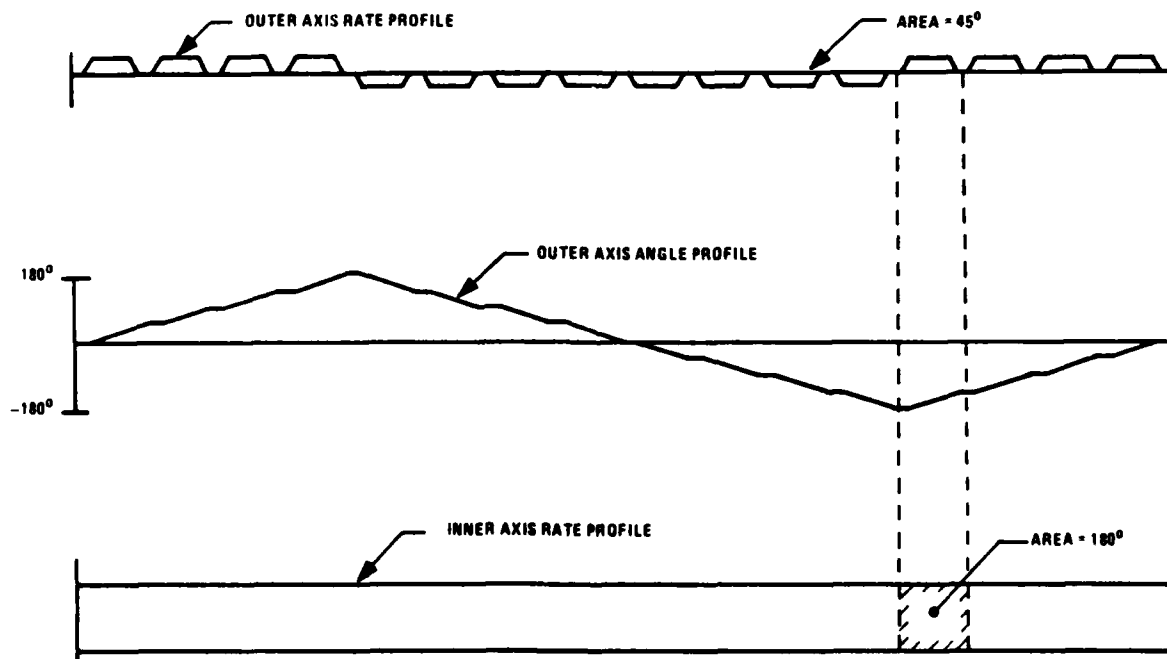


Figure 2. Dual-Freedom Sensor Assembly Rotational Profile

SECTION 3

SENSOR AND SYSTEM ERROR MODELS

GYRO RATE WHITE NOISE

The effect of rate white noise on system attitude error can be defined by the simple model:

$$\begin{aligned}\dot{\Psi} &= C_g n_g \\ &= C A n_g\end{aligned}$$

where C and A are defined by:

C = transformation matrix from sensor reference axes to local-vertical reference axes

A = transformation matrix from gyro axes to sensor reference axes

The covariance matrix of $\underline{\Psi}$ for equal intensity white noise in each gyro is governed by:

$$\dot{P} = C A A^T C^T N$$

where:

$$P = E(\Psi \Psi^T)$$

and N is the gyro white noise spectral intensity.

If, as is frequently the case, the matrix A is orthogonal, and since C is orthogonal by definition, the covariance equation reduces to:

$$\dot{P} = N$$

or:

$$P = Nt,$$

which is to say:

$$\sigma_{\psi}^2 = Nt \tag{3-1}$$

where t is the elapsed time. Therefore, rotation of the sensor assembly (implicit in C) will do nothing to reduce the effect of the gyro white noise.

SENSOR QUANTIZATION

A thorough assessment of sensor quantization errors is given in Appendix C, which defines a covariance-based model suitable for performance analysis purposes. The essence of the quantization-induced error can be described more simply by considering a single-axis rotational system. One finds that the gyro quantization error leads to an attitude random walk error, which is defined by:

$$\sigma_{\psi} = \omega \sigma_q (T/2)^{1/2} t^{1/2} \tag{3-2}$$

where:

σ_{ψ} = standard deviation of attitude error

ω = sensor assembly rotational rate

σ_q = standard deviation of the gyro quantization error

T = attitude update interval

t = time

and:

$$\sigma_q = P/\sqrt{12}$$

where P is the gyro pulse size.

A simplified analysis of the effect of accelerometer quantization leads to a formula analogous to Equation 3-2 that defines a random walk error growth in velocity.

It is clear from Equation 3-2 that the random walk error is directly proportional to rotation rate, and hence, is a major error contributor for relatively high rotation rates.

PARAMETER VARIATION

The error cancellation properties associated with any rotational strategy are applicable only when the sensor errors are constant. In reality the sensor biases, misalignments, etc., will randomly vary due to environmental and other causes.

Three types of random sensor error variations are considered below.

1. First-order Gauss-Markov process, defined by the first-order stochastic differential equation:

$$\dot{k} + \beta_1 k = \eta$$

where:

- k = random variation in the sensor error coefficient
- η = white noise
- β_1 = 1/correlation time of Gauss-Markov process

The power spectral density of the white noise input is chosen according to:

$$N_1 = 2\beta_1\sigma^2$$

where:

- N_1 = power spectral density of the white noise input
- σ = standard deviation of the steady-state sensor error variation

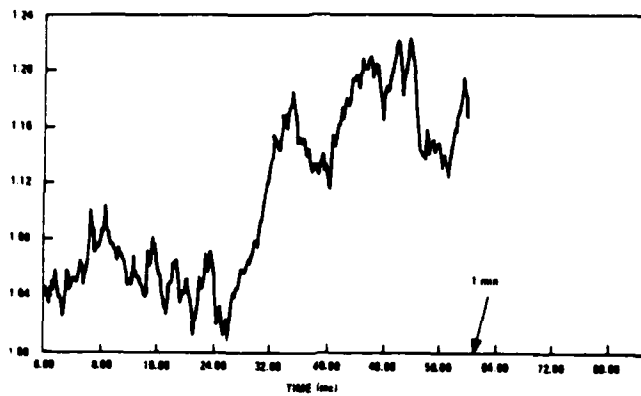
A typical sample of a first-order Gauss-Markov time history is shown in Figure 3a. The important feature is that, even for a one-hour correlation time, the response shows significant high frequency activity.

2. Second-order Gauss-Markov process, defined by:

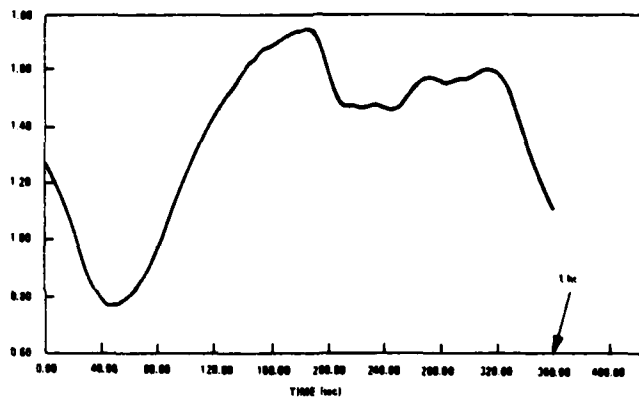
$$\ddot{k} + 2\beta_2\dot{k} + \beta_2^2k = \eta$$

where k is the error parameter variation and

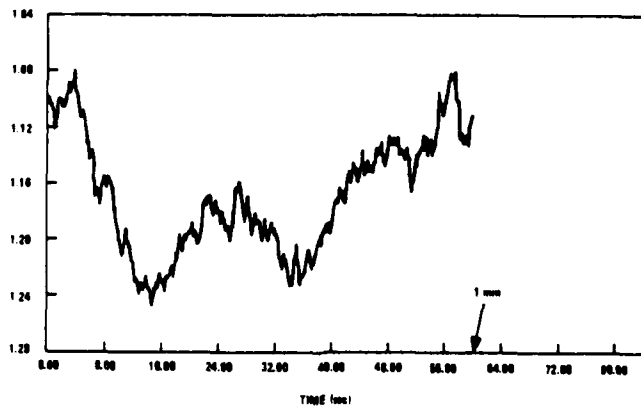
$$\beta_2 = 2.146/T_c$$



a. First-Order Gauss-Markov ($\sigma = 1$ unit, $\tau = 1$ hr)



b. Second-Order Gauss-Markov ($\sigma = 1$ unit, $\tau = 1$ hr)



c. Random Walk ($\sigma_{hr} = 1$ unit)

Figure 3. Sample Time Histories of Three Stochastic Processes

in which

T_c = correlation time of the second-order Gauss-Markov process

The spectral density of the white noise function, η , is defined by

$$N_2 = 4\beta_2^3 \sigma^2$$

where, as before, σ is the standard deviation of the steady-state sensor error variation.

A typical time history for a second-order Gauss-Markov process is shown in Figure 3b. Note that, with one-hour correlation time, the response is essentially free of all of the high frequency variations that are so prominent in the first-order Gauss-Markov process with the same correlation time.

3. A third type of random sensor error parameter variation is defined by:

$$k = \eta$$

which constitutes a random walk variation in the parameter. A sample time history for a random walk parameter variation is shown in Figure 3c. The spectral intensity of the white noise function, η , is defined by:

$$N = (\sigma_{hr}/60)^2$$

where σ_{hr} is the standard deviation of the parameter growth at one hour.

COMPLIANCE-RELATED ERRORS

In a dual-freedom strapdown system, rectified attitude drift may be generated by g-induced gyro input axis compliance effects.

Attitude error drift rate due to gyro input axis compliance may be characterized by:

$$\dot{\underline{\Psi}} = C\delta M\underline{\omega}_0^g \quad (3-3)$$

where:

$\underline{\Psi}$ = attitude error vector (with components along north-east-down (NED))

C = transformation matrix from a set of orthogonal sensor reference axes to the NED frame

δM = error in the transformation matrix from gyro input axes to the sensor reference frame

$\underline{\omega}_0^g$ = nominal angular rate vector measured by the gyro triad

The nominal angular rate vector measured by the gyros is related to the nominal angular rate vector coordinatized in the orthogonal sensor reference axes according to:

$$\underline{\omega}_0^g = M_0^{-1} \underline{\omega}_0^r \quad (3-4)$$

where:

$\underline{\omega}_0^r$ = nominal angular rate vector coordinatized in orthogonal sensor reference axes

M_0^{-1} = nominal transformation matrix from orthogonal sensor reference axes to gyro input axes

Since:

$$MM^{-1} = I$$

therefore,

$$\delta MM_o^{-1} + M_o \delta M^{-1} M_o = 0$$

and

$$\delta M = -M_o \delta M^{-1} M_o \quad (3-5)$$

Substituting Equation 3-4 and Equation 3-5 in Equation 3-3 gives

$$\dot{\underline{\Psi}} = -CM_o \delta M^{-1} \underline{\omega}_o^r \quad (3-6)$$

which is the basic attitude error equation.

To complete Equation 3-6, the following equations defining C and $\underline{\omega}_o^r$ are defined.

$$C = \begin{bmatrix} CaC\beta & -CaS\beta & Sa \\ S\beta & C\beta & 0 \\ -SaC\beta & SaS\beta & Ca \end{bmatrix} \quad (3-7)$$

$$\underline{\omega}_o^r = (\dot{\alpha} \sin \beta t \quad \alpha \cos \beta t \quad \beta)^T \quad (3-8)$$

where:

α = outer gimbal angle

β = inner gimbal angle

For a gyro triad whose axes are nominally orthogonal and coincident with the sensor assembly reference axes:

$$M_0 = I \quad (3-9)$$

and the error in M_0^{-1} can be expressed in general by:

$$\delta M^{-1} = \begin{bmatrix} 0 & \delta a_1 & \delta b_1 \\ \delta a_2 & 0 & \delta b_2 \\ \delta a_3 & \delta b_3 & 0 \end{bmatrix} \quad (3-10)$$

where δa_i and δb_i are the gyro input-axis misalignment angles.

Now assume that each misalignment angle error can be defined in terms of the three components of gravity in the orthogonal sensor reference frame according to:

$$\delta a^i = k_{i1} A_1^r + k_{i2} A_2^r + k_{i3} A_3^r \quad (3-11)$$

$$\delta b_i = m_{i1} A_1^r + m_{i2} A_2^r + m_{i3} A_3^r \quad (3-12)$$

where the k_{ij} and m_{ij} are compliance coefficients, and A_1^r , A_2^r , and A_3^r are the components of the gravity reaction acceleration, defined from Equation 3-7 by:

$$A^r = -g(-\text{SaCb} \text{ SaSb} \text{ Ca})^T$$

where g is the acceleration due to gravity.

Substituting Equations 3-7, 3-8, 3-9, 3-10, 3-11, and 3-12 into Equation 3-6 yields an attitude error equation that takes the following form.

$$\dot{\underline{\Psi}} = \underline{f} (\alpha, \beta, \dot{\alpha}, \dot{\beta}, k_{11}, k_{12}, \dots, m_{11}, m_{12}, \dots, t)$$

where:

$$\underline{\Psi} = (\Psi_n \Psi_e \Psi_d)^T$$

and all terms in the linear expansion have either $\dot{\alpha}$ or $\dot{\beta}$ as a multiplier.

Each component of $\underline{\Psi}$ can be determined at the end of a complete gimbal period by direct integration of $\dot{\underline{\Psi}}$. In the process of doing this, one can easily eliminate terms involving α by inspection. For example, a term such as

$$\int_0^t \dot{\alpha} \sin \alpha t \cos \beta t \, dt$$

is identically zero at the completion of every outer gimbal 360° traversal (of duration T), while a term such as

$$\int_0^t \beta \sin^2 \beta \, dt$$

has a non-zero mean value at the end of each outer axis period.

SECTION 4

SYSTEM ERROR STUDIES

ERROR PROPAGATION IN DUAL-FREEDOM SYSTEM

In a rotating system, error propagation depends on the nature of the random sensor errors. For example, consider the simplified block diagram shown in Figure 4 for attitude error propagation in a single-freedom system. The variance of the attitude error can be determined from:

$$\sigma_{\Psi}^2(t) = N \int_0^t w^2(t, \tau) dt$$

where:

$w(t, \tau)$ = response of the system at time t to an impulse applied at time τ

N = power spectral density of the white noise input

σ_{Ψ}^2 = variance of the attitude error

For the first-order Gauss-Markov process, the impulse response function is given by:

$$w(t, \tau) = \int_0^t e^{-\beta_1(t-\tau)} \sin \omega \tau d\tau$$

and for the second-order Gauss-Markov process:

$$w(t, \tau) = \int_0^t (t-\tau) e^{-\beta_2(t-\tau)} \sin \omega \tau d\tau$$

For the random walk process:

$$w(t, \tau) = \int_0^t U(\tau) \sin \omega \tau d\tau$$

where U denotes the unit step function.



a. First-order Gauss-Markov process



b. Second-order Gauss-Markov process



c. Random-walk process

- η = UNIT INTENSITY WHITE NOISE
- σ = STANDARD DEVIATION OF GYRO BIAS VARIATIONS IN STEADY STATE (GAUSS-MARKOV PROCESS)
- ω = ROTATION FREQUENCY
- ψ = ATTITUDE ERROR
- β_1 = 1/(CORRELATION TIME OF FIRST-ORDER GAUSS-MARKOV PROCESS)
- β_2 = 2.146/(CORRELATION TIME OF SECOND-ORDER GAUSS-MARKOV PROCESS)
- σ_{hr} = STANDARD DEVIATION OF GYRO BIAS VARIATION AT 1 hr (RANDOM WALK PROCESS)

Figure 4. Attitude Error Propagation in a Rotational System

The asymptotic characteristics of the solutions can be established by carrying out the integrations analytically and discarding all terms in the solution that decay with time. The result is that the attitude error variances become asymptotically equal to:

$$\sigma^2 = \phi_1(\omega)t/2 \quad (\text{first-order Gauss-Markov}) \quad (4-1)$$

$$\sigma^2 = \phi_2(\omega)t/2 \quad (\text{second-order Gauss-Markov}) \quad (4-2)$$

where $\phi_1(\omega)$ is the power spectral density of the first-order Gauss-Markov process at the rotational frequency, ω , and is defined by:

$$\phi_1(\omega) = \frac{2\beta_1\sigma^2}{\beta_1^2 + \omega^2}$$

and $\phi_2(\omega)$ is the power spectral density of the second-order Gauss-Markov process at the rotational frequency, and is given by:

$$\phi_2(\omega) = \frac{4\beta_2^3\omega^2}{(\beta_2^2 + \omega^2)^2}$$

For the random walk parameter variation

$$\sigma^2 = \phi_r(\omega)t$$

where:

$$\phi_r(\omega) = (\sigma_{hr/60})^2/\omega^2 \quad (4-3)$$

It is seen, therefore, that all three processes lead to a random walk error propagation tendency in attitude. It is also clear that, for the Gauss-Markov processes, the variance of the random-walk component of attitude error is directly proportional to the amount of power in the process at the rotational frequency, ω . Comparing ϕ_1 and ϕ_2 , the ratio of powers at the rotational frequency is determined as

$$\phi_1(\omega)/\phi_2(\omega) = \frac{\beta_1}{\beta_1^2 + \omega^2} \cdot \frac{(\beta_2^2 + \omega^2)^2}{2\beta_2^3} = \frac{\beta_1(\beta_2^2 + \omega^2)^2}{2\beta_2^3(\beta_1^2 + \omega^2)}$$

For example, consider:

$$\beta_1 = 1/1800$$

$$\beta_2 = 2.146/1800$$

$$\omega = 2\pi/60$$

which yields the result that

$$\theta_1(\omega)/\theta_2(\omega) = 1799$$

Therefore, the standard deviation of the random walk component is greater by a factor of $\sqrt{1799} = 42.4$ for the first-order Gauss-Markov process compared to the second-order Gauss-Markov process for the example chosen.

It is clear from Equations 4-1, 4-2, and 4-3 that each type of parameter variation leads to a random-walk in attitude. It can be shown that, for a Gauss-Markov process of any order whatsoever, the attitude error growth is defined by the general form:

$$\sigma_\Psi^2 = \theta_N(\omega)t/2$$

where $\theta_N(\omega)$ is the power spectral density of the n^{th} -order Gauss-Markov process at the rotational frequency ω . The implication is that the choice of a random process for representing sensor variations is not critical. It is important only that the power at the rotational frequency have some meaningful value. This is true for performance analyses and for Kalman filter design and evaluation.

COVARIANCE ANALYSIS AND KALMAN ESTIMATION

Consider a dynamic system whose behavior is defined by the following set of discrete linear equations:

$$X_n = \theta_n X_{n-1} + B_n \eta_n \tag{4-4}$$

where:

X = vector of states

η = vector of random (zero mean) noise sequences

Φ_n = state transition matrix from (n-1)th to nth iterations

B_n = noise distribution matrix at the nth iteration

For a given Φ and B , the state X will have a time variation determined by the particular noise sequence, η , and the initial condition, X_0 , which in general is taken to be a randomly distributed quantity. Since the noise sequence, η , has an infinite number of realizations and the initial condition error can assume an infinite number of values, the system of equations given by Equation 4-4 has an infinite number of solutions. Because this is true, attention must be focused on the statistical behavior of Equation 4-4 rather than on specific solutions.

The most natural and useful way of characterizing the behavior of Equation 4-4 is to compute the statistical parameters that define the bounds on the state vector, X . The statistical bounds on the components of X are found by solving the covariance matrix equation associated with Equation 4-4, which takes the recursive form:

$$P_n = \Phi_n P_{n-1} \Phi_n^T + B_n Q_n B_n^T \quad (4-5)$$

where P is the state covariance matrix of the state vector, X , defined explicitly by:

$$P = [p_{ij}]$$

and

$$p_{ij} = E(X_i X_j)$$

in which E denotes the expectation operator. It is seen that the individual variances of the components of X are defined by the diagonal elements of P , with the joint expectancies (cross-correlations) being defined by the off-diagonal elements of P . The matrix Q in Equation 4-5 is the covariance matrix of the driving noise vector, η , which is defined by:

$$Q = [q_{ij}]$$

and

$$q_{ij} = E(\eta_i \eta_j)$$

Suppose that the discrete process defined by Equation 4-4 represents the true dynamic propagation characteristics of a given linear system. Suppose further that at some time a measurement is made (using an external measuring device) that allows a specific linear combination of the states to be directly monitored. A generalized way of stating this in mathematical form is

$$Y_m = H_m X + \xi_m \tag{4-6}$$

where:

Y_m = vector of measurements at time t_m

H_m = measurement matrix at time t_m

ξ_m = measurement noise vector applicable to m^{th} measurement

and it is assumed, in the general case, that a number of independent measurements may become available simultaneously.

Consider now the question of how one could use the information introduced through a series of measurements of the form given by Equation 4-6 to optimally estimate the state X in a sequential fashion. This is the central problem addressed by Kalman estimation theory, and has the following solution.

After each measurement (of a sequence of measurements) is made, the estimate of the state X is refreshed by the two-step procedure:

$$\hat{X}^-(t_m) = \Phi(t_m, t_{m-1}) \hat{X}^-(t_{m-1}) \quad (4-7)$$

$$\hat{X}(t_m) = \hat{X}^-(t_m) + K_m (Y_m - H_m \hat{X}^-(t_m)) \quad (4-8)$$

where:

$\hat{X}^-(t_m)$ = best estimate of vector X just prior to the m^{th} measurement

$\hat{X}(t_m)$ = best estimate of vector X after incorporating the information introduced by the m^{th} measurement

$\Phi(t_m, t_{m-1})$ = state transition matrix spanning the time between the m^{th} and $(m-1)^{\text{th}}$ measurements

K_m = Kalman gain matrix at the m^{th} measurement point

Y_m = vector of measurements

H_m = measurement (observation) matrix at m^{th} measurement

with K_m defined by:

$$K_m = P_m^- H_m^T (H_m P_m^- H_m^T + R_m)^{-1} \quad (4-9)$$

in which

P_m^- = a priori error covariance matrix of the vector X

R_m = measurement error covariance matrix = $E(\xi_m \xi_m^T)$

and the a priori error covariance matrix P_m^- is computed by using Equation 4-5 over the period from the m^{th} to $(m-1)^{\text{th}}$ measurements.

After processing of the m^{th} measurement, the error covariance matrix of the state X is modified to reflect the benefit of incorporating the new information introduced by the measurement, as follows.

$$P_m = (I - K_m H_m) P_m^- \quad (4-10)$$

and P_m is referred to as the "a posteriori" error covariance matrix. The form given by Equation 4-10 is applicable when the Kalman filter is fully optimal; that is, the filter is a full-state filter in which all components of X are fully accounted for in the mathematic model, and further, are re-estimated after each successive measurement is made available.

Formulation of Dual-Freedom System Simulation

The northfinding process is assumed to take place in real-time (rather than by data post processing) via optimal estimation (Kalman filtering) techniques. The alignment Kalman filter is based on the fact that the reference origin of the sensor assembly has zero velocity. Then, the velocity indicated by the system becomes a measure of the alignment errors (azimuth and level).

A discrete error equation for expressing deviations in attitude and velocity for the northfinding mode is given as (see Appendix B):

$$\underline{Y}_n = \phi_{11} \underline{Y}_{n-1} + \phi_{12} \underline{X}_{n-1} + \underline{\xi}_n \quad (4-11)$$

where \underline{Y} is the vector of attitude and velocity error states defined by:

$$\underline{Y} = (\underline{\Psi} \ \underline{\delta V})^T \quad (4-12)$$

in which:

$\underline{\Psi}$ = attitude error vector

$\underline{\delta V}$ = velocity error vector

and \underline{X} is the vector of sensor errors, which are represented in general by second-order Gauss-Markov processes:

$$\underline{X} = (X_1 \ X_2 \ \dots \ X_N)^T \quad (4-13)$$

Each component of the sensor bias vector, \underline{X} , is defined by two first-order differential equations according to (see Figure 4b):

$$\dot{X}_i + \beta_2 X_i = U_i \quad (4-14)$$

$$\dot{U}_i + \beta_2 U_i = \sqrt{4\beta_2^3} \eta \quad (4-15)$$

where η is a unit intensity white noise function, and

$$\beta_2 = 2.146/(\text{correlation time})$$

The vector \underline{X} represents the short-term instability in the sensor error parameter vector. Only the short-term instability is of importance. The constant components of sensor error are dealt with by the error commutation properties inherent in the sensor assembly rotational profile (see Figure 2). The single exception is vertical drift rate, due to input-axis compliance. Since this effect is highly stable over time (based on experimental evidence), it is assumed that, prior to northfinding, the vertical drift rate has been calibrated and compensation provided. Alternatively, the vertical drift rate may be fine-calibrated during the northfinding process by adding an additional state to the Kalman filter. In either case, the effect of the vertical drift rate can be made negligibly small.

Equations 4-11 through 4-15 describe the evolution of the error state. The discrete uncorrelated process noise vector, \underline{g} , is defined to include gyro random walk and sensor quantization errors.

The measurement equations for the northfinding process are defined by:

$$y_1 = \delta V_1 + \mu_1 \quad (4-16)$$

$$y_2 = \delta V_2 + \mu_2 \quad (4-17)$$

where:

y_1, y_2 = indicated velocity outputs of the navigation system along north and east axes, respectively

$\delta V_1, \delta V_2$ = errors in the north and east velocity components, respectively

μ_1, μ_2 = measurement errors (spurious velocity components due to random base motion effects)

Based on Equations 4-11 through 4-17, an alignment Kalman filter is defined. In the present study, the Kalman filter update interval is chosen to be the same as the period of the outer axis rotational profile (4 min). By so doing, the achievable alignment accuracy becomes independent of any latent sensor calibration errors. Only short-term instabilities in the sensor errors (as defined by Equations 4-14 and 4-15) affect the accuracy of the alignment. By enforcing this constraint, the computational requirements of the alignment Kalman filter are greatly reduced, without loss of performance.

A set of 1 σ sensor errors that was assumed for assessing the performance of the three-axis navigator approach is defined in Table 1. The gyro random walk coefficient of $.45 \times 10^{-4}$ deg at 1 hr is based on experimental results obtained for the Honeywell GG1389 laser gyro. The quantization 1 σ errors are based on the assumption of a uniform distribution for the quantization error, and the use

TABLE 1. 1σ ERRORS ASSUMED FOR THREE-AXIS SIMULATION

<u>Gyro</u>	
•	Random walk = $0.000045^\circ/\sqrt{\text{rt-hr}}$
•	Quantization = 0.022 arc-sec
•	Gyro bias short-term variation = $0.01^\circ/\text{hr}$
•	Gyro scale factor short-term variation = 0.05 ppm
•	Gyro input axis misalignment short-term variation = 0.05 arc-sec
<u>Accelerometer</u>	
•	Quantization = 0.0006 ft/sec
•	Accel bias short-term variation = 0.10 micro-g
•	Accel scale factor short-term variation = 0.5 ppm
•	Accel input axis misalignment short-term variation = 0.5 arc-sec
<u>Other</u>	
•	Short-term translational base motion = 0.005 ft/sec

of a phase-lock loop to increase the resolution of the gyro output to 0.075 arc-sec.

The short-term sensor errors are assumed to be second-order Gauss-Markov processes with a correlation time of 1 hr. However, the 1σ values given in Table 1 are not meant to imply bounded behavior. Rather, the intent is to characterize their short-term variation over times comparable to the period of the outer axis (4 min in this case).

Results of Dual-Freedom System Simulation

The three-axis system covariance and error sensitivity analyses were first framed around the assumption of using three GG1300 RLGs, with a complete set of rms error parameter values assumed as below. Errors are assumed random independent, and with Gaussian distributions, except for quantization errors, which are assumed to be sum-bounded, and to have triangular distributions.

Gyro: Honeywell GG1300 RLGs, in rate-biased mode (i.e., prolonged unidirectional rotation)

Angle random walk	0.0001°/rt-hr
Quantization/spillover	0.03 arc-sec
Bias random walk	0.01°/hr-rt-hr
Scale factor random walk	0.05 ppm/rt-hr

Accelerometers: 3 Bell 11s, or equivalent

Pulse-weight quantization	0.0006 ft/sec
Acceleration random walk	0.1 micro-g's/rt-hr
Scale factor random walk	0.5 ppm/rt-hr
Input axis instability	0.5 arc-sec/rt-hr

Bias errors are cancelled by carouseling around two indexation axes, over a 4-min cycle. Consequently, the system puts out updates of three-axis attitude 15 times per hour. At each update, the system output is reset, by "reminding" the system computations that the system has undergone zero displacement over the preceding 4 min, and has zero velocity.

The reset process is clearly seen in Figure 5, which shows the evolution of rms drift error around the north-south axis, as produced by computer simulations. The error locus is the lower envelope, with an asymptotic value of about 0.085 arc-sec. The simulation is quite similar for east-west axis drift. In Figure 6, we see the simulation of vertical axis drift error. This has an apparent asymptote of about 1.4 arc-sec. The drift is smaller around the horizontal axes because the gyros are greatly helped by the tiltmeter aspect of the accels. Horizontal axis drift is dominated by the accel quality and vertical axis drift by the gyro quality.

The Honeywell GG1300 RLG, on which the foregoing results were obtained, used to be our best gyro. Now, we have the high-performance GG1389 RLG, with the following characteristics:

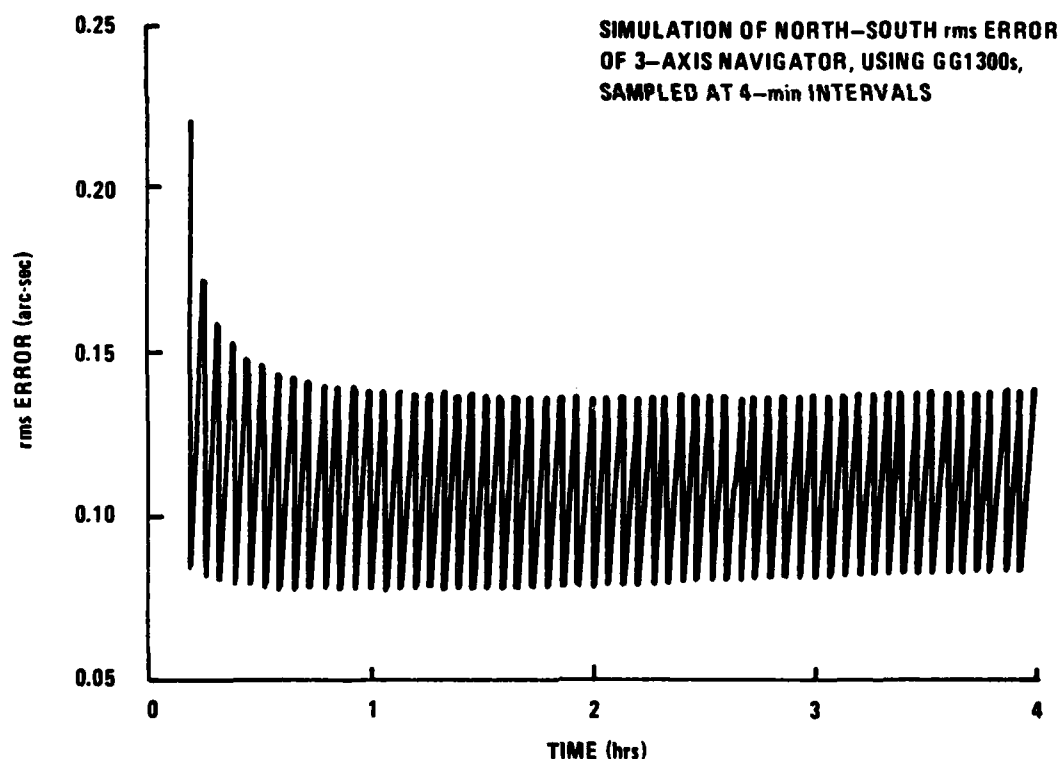


Figure 5. Simulated North-South rms Error, Using GG1300s

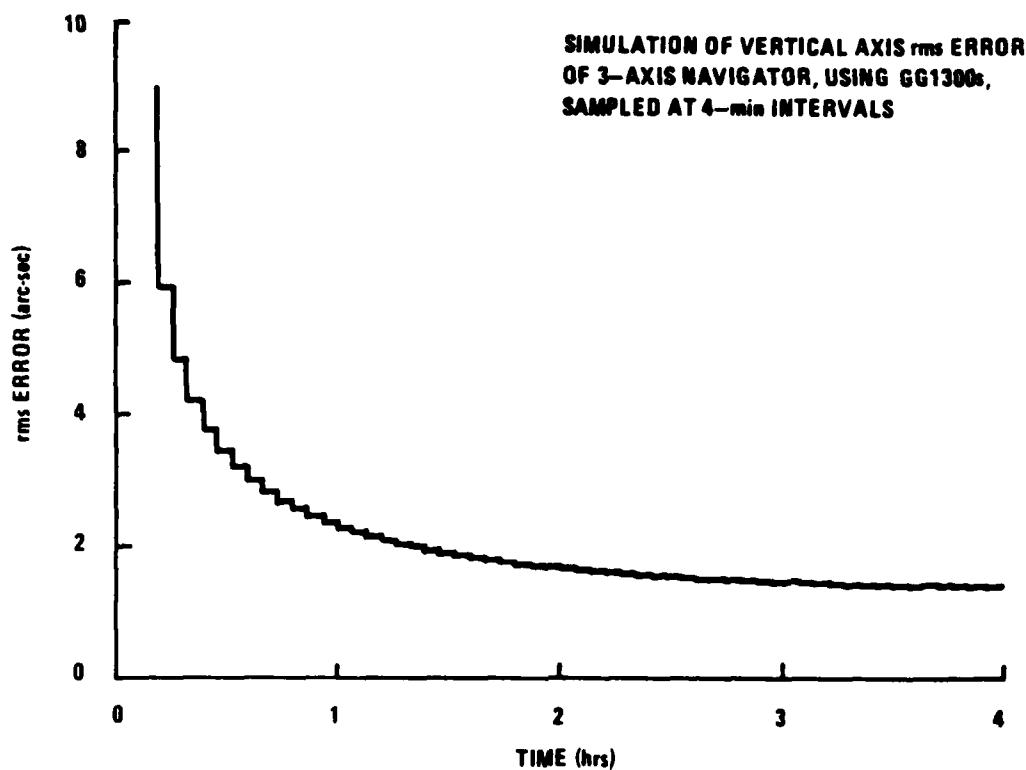


Figure 6. Simulated Vertical rms Error, Using GG1300s

Gyro: Honeywell GG1389 RLG, in rate-biased mode (i.e. prolonged unidirectional rotation)

Angle random walk	0.000045°/rt-hr
Quantization/spillover	0.02 arc-sec
Bias random walk	0.01°/hr-rt-hr
Scale factor random walk	0.05 ppm/rt-hr
Input axis instability	0.05 arc-sec/rt-hr

We see from Figures 7 and 8 that the simulations show drift errors around the east-west and north-south axes of about 0.075 arc-sec. This is about the same as with GG1300s. As previously mentioned, this part of the drift is accel-limited. In Figure 9 we see that drift around the vertical is asymptotically 0.55 arc-sec; as could be expected, this gyro-limited term is improved by going from the GG1300 to the GG1389. However, it is still too high for a subarc-second system.

Discussion of Simulation Results

The reason that the vertical axis drift is asymptotically bounded (rather than being an unbounded random drift to match the unbounded random walk of the vertical component of the gyro outputs), is as follows: The vertical axis drift attempts to "tell" the system that the horizontal gyro sensing plane is in unbounded rotation. If this were really so, then the direction of the horizontal component of earth rate, as seen by the system, should also appear to be unboundedly rotated. When this fails to occur, the system starts to "ignore" the vertical axis drift. The final result is a compromise between vertical axis random angle drift and horizontal plane angular rate white noise.

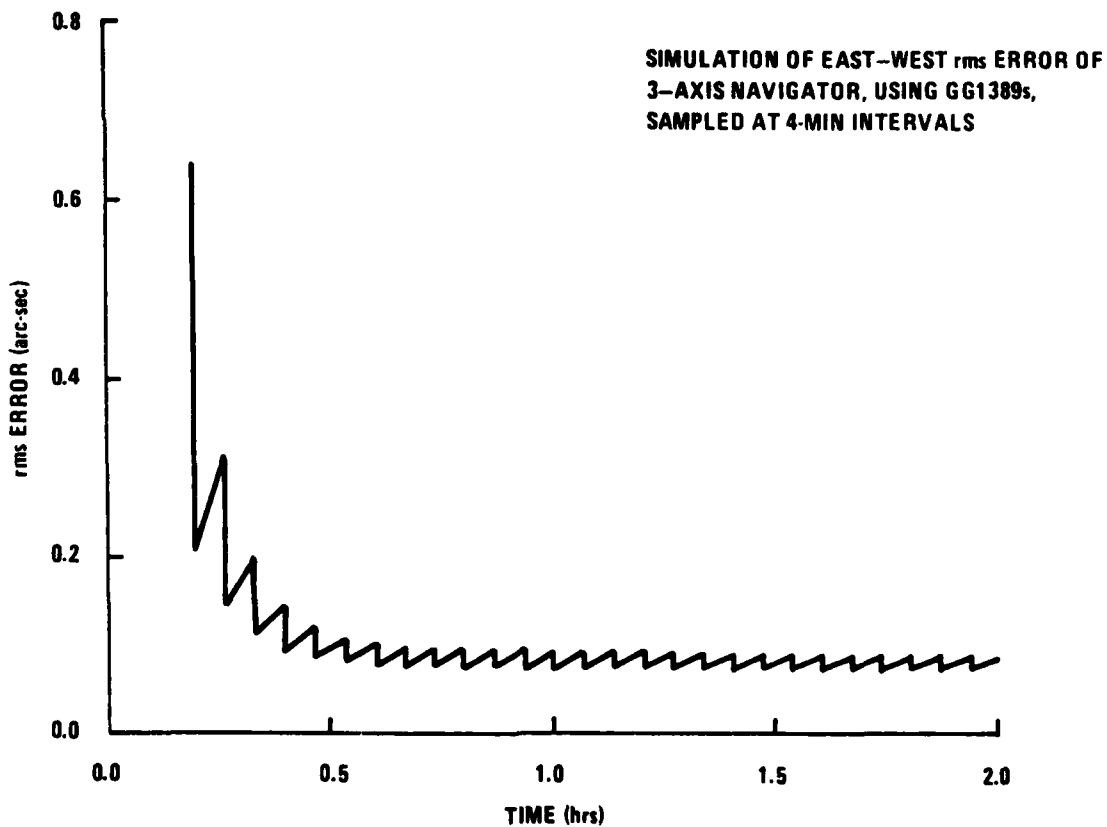


Figure 7. Simulated East-West rms Error, Using GG1389s

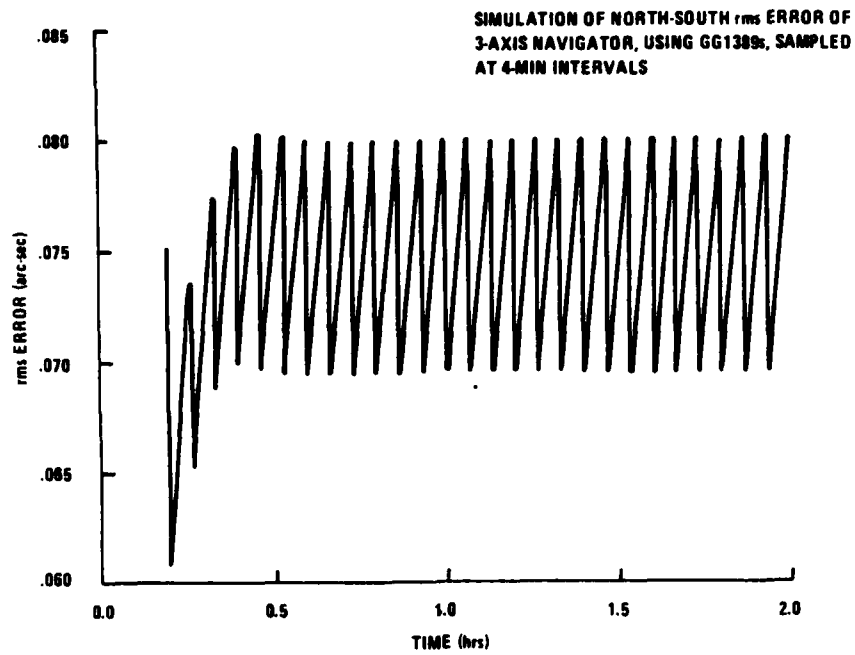


Figure 8. Simulated North-South rms Error, Using GG1389s

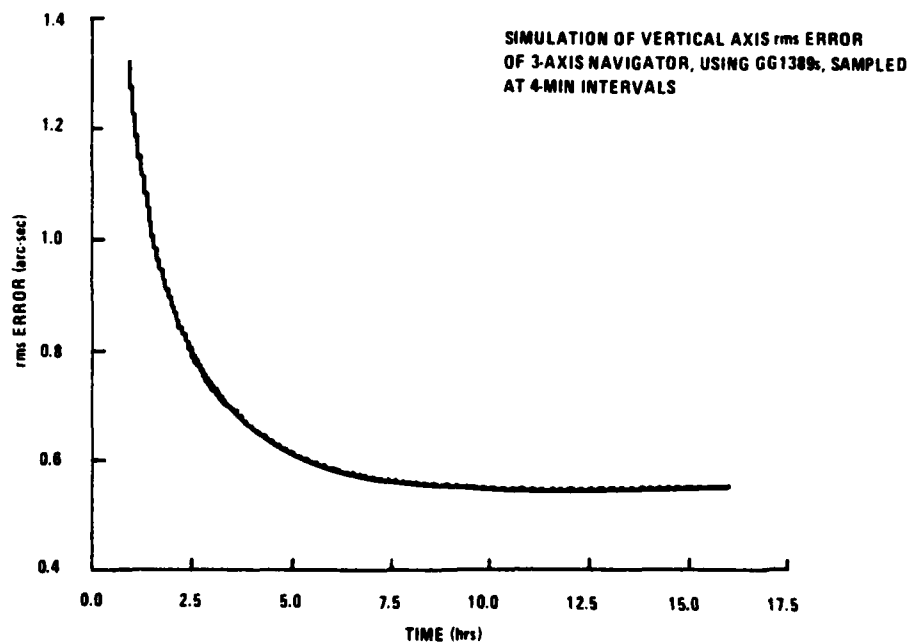


Figure 9. Simulated Vertical rms Error, Using GG1389s

The azimuth error is estimated via the two horizontal velocity components, and this process tends to follow the law

$$\sigma_{\psi} = \frac{N^{1/2} t^{-1/2}}{\omega_e c\lambda} \quad (4-18)$$

where

N = intensity of gyro white noise drift

ω_e = earth's rotational rate (0.729×10^{-4} rad/sec)

$c\lambda$ = cosine of latitude

σ_{ψ} = 1 σ error in estimated azimuth

Simultaneously, the azimuth error tends to grow due to the component of total gyro random drift acting in the vertical direction. This increase in azimuth error follows the law

$$\sigma_{\psi} = N^{1/2} t^{1/2} \quad (4-19)$$

Therefore, the decay of error, as predicted by Equation 4-18, is equal to the growth of error predicted by Equation 4-19 when:

$$\frac{1}{\omega_e c\lambda t^{1/2}} = t^{1/2}$$

or when

$$t = \frac{1}{\omega_e c\lambda}$$

For $\lambda = 45^\circ$, this gives:

$$t = 19402 \text{ sec} = 5.4 \text{ hr}$$

This is reasonably close to the azimuth error convergence time constant seen in Figure 9. The basic reason we see this irreducible azimuth error is that the overall model included the possibility of azimuth drift over the measurement period.

If one assumes that the system maintains an essentially fixed orientation relative to north over an indefinite time, further accuracy of northfinding is possible. A simple approach would be to average a series of northfinding results, each obtained over some fairly short period of time (say about 1/4 hr). Then, the composite accuracy would be improved by a factor equal to the square root of the total measurement time. If, as an example, 64 northfinding experiments were run, each 1/4 hr, then the composite accuracy would be:

$$\sigma_{\psi} = 1.3/4 = 0.32 \text{ arc-sec}$$

This is the basis of the simplified one-axis concept, measuring over a 16-hr interval. Assuming constant orientation relative to north, the composite accuracy of a sequence of northfindings would improve indefinitely. Thus, at 48 hr, the 1σ azimuth error would be 0.20 arc-sec, and so on.

SECTION 5

ONE-AXIS SYSTEM STUDY

ERROR ANALYSIS

The results of the three-axis navigator system studies suggest that it is pointless to measure rate around the vertical axis. We need a different approach and philosophy. In the horizontal plane, the best quality earth-rate information is conveyed along the east-west axis. Earth-rate measured around the north-south axis is maximum for horizontal axis measurements, and hence varies only second-order with first-order azimuthal drift, i.e., conveys zero azimuthal drift information. Thus, we are led to the concept of using a single gyro, oriented east-west. This is the basis of the one-axis alternate system.

Because of the rather simple theoretical structure, error effect analyses are straightforward, the hardest part is deciding on a model of the kinds of errors to consider. For completeness, we assume that there are random errors in measuring the g , the g' , and the e vectors, not necessarily uncorrelated. There are seven variable errors to consider, namely, in e_1 , e_2 and e_3 , in g_1 and g_2 , and in g'_1 and g'_2 . g_3 is assumed to vary only second-order around its nominal value of 1, and isn't measured. g'_3 , the time derivative of g_3 , is of course also second order and is ignored.

It is convenient to discuss errors in terms of their main end effects. In this case, the obviously crucial end effect is the misdefinition of the earth-fixed reference frame, described by the orthogonal triad i , j , and k , along east, north, and upward vertical. The error end effect comprises small increments, di , dj , and dk , respectively perpendicular to i , j , and k . The i , j , and k axes are constructed from the computed wander-corrected unit vector earth spin axis, s , and from the computed unit vertical vector, v . For k , we use v . Knowing the latitude, L , we express s as:

$$s = j \cdot \cos(L) + k \cdot \sin(L)$$

For j , we use the k -free component of s , normalized to unity:

$$j = (s - k \cdot (k \cdot s)) / \cos(L)$$

(where ' $k \cdot s$ ' denotes 'scalar product of vectors k and s '')

For i , we simply vector-crossproduct j and k :

$$i = (s \times k) / \cos(L)$$

The error in k is simply the error in v , conveniently expressed as

$$dk = dv = i \cdot v_1 + j \cdot v_2$$

The error in s is conveniently expressed in terms of east-west and meridional components, along i and along $k \cdot \cos(L) - j \cdot \sin(L)$, respectively:

$$ds = i \cdot s_1 + (k \cdot \cos(L) - j \cdot \sin(L)) \cdot s_2$$

The errors in i , j , and k , in terms of dv and ds are

$$di = ((ds \times k) + (s \times dv)) / \cos(L)$$

$$dj = (ds - dv \cdot (k \cdot s) - k \cdot (dv \cdot s) - k \cdot (k \cdot ds)) / \cos(L)$$

$$dk = dv$$

These effects can be represented by a rotational error vector, z:

$$d_i = z \times i$$

$$d_j = z \times j$$

$$d_k = z \times k$$

where:

$$z = -i \cdot v_2 + j \cdot v_1 + k \cdot (v_1 \cdot \sin(L) - s_1) / \cos(L)$$

The reference-frame errors depend on the two components, v_1 and v_2 , of the vertical error and on the east-west component, s_1 , of the earth spin axis error. Since the meridional component of the earth spin is ignored, by relying solely on the north-south component of the tiltmeters, s_2 plays no role in the error analysis. The rationale for so doing is the assumption that the tiltmeter accuracy will be considerably better than the gyro accuracy, so any inconsistency between tiltmeter readings and gyro readings (implying a false value of latitude) is to be resolved in favor of the tiltmeters.

The error components v_1 , v_2 , and s_1 are simply:

$$v_1 = \text{err}(a_2) = \text{err}(g_1)$$

$$v_2 = \text{err}(-a_1) = \text{err}(g_2)$$

$$s_1 = -\text{err}(d_1/R)$$

$$= \sin(L) \cdot \text{err}(g_1) - \cos(L) \cdot \text{err}(a_3) - (\text{err}(e_1) + \text{err}(g'_2)) / R$$

Substituting, the rotational error vector becomes:

$$z = -i \cdot \text{err}(g_2) + j \cdot \text{err}(g_1)$$

$$+ k \cdot (\text{err}(a_3) + (\text{err}(e_1) + \text{err}(g'_2)) / (R \cdot \cos(L)))$$

If we use independently-generated values of earth spin axis deviation, or multi-site averaging of vertical axis warp, we dispense with the theodolite observations of landmarks, and the a3 contribution to z disappears, giving:

$$z = -i*err(g2) + j*err(g1) + k*(err(e1) + err(g'2))/(R*cos(L))$$

This says that the tilt component of the rotational error (i.e., that part which is around a horizontal axis), is due to the tilt measurement error (crossproducted with the unit vertical), and that the azimuthal rotation component is due to east-west axis rotational error, comprised of the sum of gyro east-west axis rate measurement error and of east-west axis rate-of-tilt measurement error. The foregoing results are completely in harmony with intuition. The components of z around horizontal axes are governed simply and solely by the tiltmeter errors. The component of z around the vertical axis has the expected sensitivity to latitude. The errors in g1 and g2 are respectively east-west and north-south tilt errors, and that in g'2 is the error in determining the rate of change of north-south tilt. The error in e1 is the error in measuring east-west rate.

GYRO PERFORMANCE REQUIREMENTS

Assume the performance is to be dominated by gyro random drift error. This is justified by the high-quality state of the art in tiltmeters and by the fact that we can remove the effect of gyro low frequency bias errors by indexing (as well as tiltmeter bias effects). Then, the azimuthal component of the error vector, z, will be equal to:

$$z(az'l) = err(e1)*secant(latitude)/earthrate$$

The rms error in ϵ_1 will, under angle random walk (which is rate white noise), be equal to the random walk coefficient divided by the square root of the time of observation, giving:

$$z(\text{az}'1) = \text{RW} * \text{SEC}(L) / (\text{R} * \text{SQRT}(\text{TAU}))$$

where:

RW = Random drift coefficient, deg/rt-hr

L = Latitude

R = Earthrate, deg/hr

TAU = Time of observation, hr

Putting $R = 15.0411^\circ/\text{hr}$, and assuming a measurement time of 16 hr, and converting $z(\text{az}'1)$ from radians to arc-seconds:

$$\begin{aligned} z(\text{az}'1) &= 206265 * \text{RW} * \text{SEC}(L) / (15.0411 * 4) \\ &= 3428 * \text{SEC}(L) * \text{RW} \text{ arc-sec rms} \end{aligned}$$

Assuming that we want $z(\text{az}'1) = 0.2$ arc-sec, the random walk value needed to achieve this is

$$\begin{aligned} \text{RW} &= 0.2 * \text{COS}(L) / 3428 \\ &= 0.000058 * \text{COS}(L) \text{ deg/rt-hr} \end{aligned}$$

Thus, at the equator, we need a 0.000058 gyro. At latitude 45° , 0.00004 would be needed.

EXPECTED SYSTEM PERFORMANCE

The finite effects of bias instability and quantization are considered explicitly as follows. With indexed readings taken over total time T, with each indexed reading lasting time t, the total rms error angular error is given by the expression:

$$\text{SQRT}(\text{QS}^2/(t \cdot T) + \text{RW}^2/T + 3 \cdot (\text{BI} \cdot t/T)^2) / (R \cdot \text{COS}(LT))$$

where:

QS = rms quantization/spillover	= 0.024 arc-sec
RW = Random walk coefficient	= 0.00004°/rt-hr
BI = Low frequency bias instability	= 0.0003°/hr
R = Earth rate	= 15.041°/hr
LT = Latitude	= 45°
T = Total measurement time	= 16 hr
t = Indexation period	

The gyro parameter values are from the experimental undithered gyro data reported in Section 6. The only assumption is that dithered operation can be enhanced to give the same random walk as undithered operation, using closed-loop lockin correction (CLIC) to cancel out random errors accrued at each dither reversal, as discussed in a later subsection (Gyro Modifications Needed).

Using the above numerical values, the rms error in arc-sec, as a function of t, is given by:

$$\text{rms error} = \text{SQRT}(0.001/t + 0.038 + 0.4 \cdot t^2)$$

This has a minimum value of 0.23 arc-sec at t = 0.11 hr. Therefore, the optimum indexation rate is about 9 times per hour.

HARDWARE REQUIREMENTS

Since only the e1 component of rate error matters, it makes sense to minimize e1 by using all the time available to take east-west rate readings. This suggests that we need only an east-west gyro. An added benefit of using the gyro along a nominally null-rate axis is that gyro scale-factor variability is not an issue. Similarly, tiltmeter scale factor variability is removed from the picture by installing the tiltmeters nominally horizontal.

Factors contributing to the error in determining the e1 component of the earth spin vector are gyro bias error and gyro input axis error, as follows:

$$\text{err}(e1) = dB + R*(dV*\sin(L) + dH*\cos(L))$$

where:

dB = Deviation of gyro bias rate from nominal

dV = Vertical deviation of gyro axis from nominal

dH = Horizontal deviation of gyro axis from nominal

If the deviations, though unknown, are constant over the observation period, we can cancel their effects by taking indexed readings, pointing first east, then west, and evaluating the east axis rate as the averaged east reading, minus the averaged west reading, divided by 2. Indexing around the vertical axis will cancel the error contributions from dB and dV. Indexing around the north-south axis will cancel the error contributions from dB and dH. If the deviations are time-variant, the benefits of indexing will depend on the dynamics of the time variation.

High frequency bias variation is exemplified by ordinary gyro angle random walk i.e., rate white noise, against which indexing has no effect. Hence, gyro output angle random walk is a major driver in this application. Laser gyro

input axis variation is believed to be of order 1 arc-sec and to vary very slowly, with a time constant of hours, at least. Thus, indexing should greatly dilute the δV contribution, probably to a negligible level.

Indexing introduces its own set of added errors, corresponding to the accuracy and repeatability with which the indexed orientations are achieved. The ULTRADEX commercial indexing device can index back and forth through 180° with error of $< 1/8$ arc-sec and repeatability better than $1/20$ arc-sec, around the index axis. The tilt error is ostensibly of order 1 to 2 arc-sec, and is some variable blend of random from one index to the next and/or quasi-constant.

Any random component would be attenuated over N successive indexes, by a factor of $\text{SQRT}(N)$. Also, it ought to be possible to directly measure the tilt of the ULTRADEX'd upper surface (bearing the gyro and tiltmeters) relative to the lower main stationary surface on which the ULTRADEX rests. In principle, sensitive height gages could measure the elevation of the upper surface over the lower, at four equi-spaced points around the rim of the upper surface. A trivial calculation would yield the two-axis relative tilt.

GYRO MODIFICATIONS NEEDED

With only one gyro, it is impractical to use kinematics such as are used in the three-axis system. Three-axis rate information is a must for tallying compound rotation. A one-axis system must keep the gyro in fixed, or highly constrained, orientations to avoid uncomputability situations. But, the whole point of the three-axis kinematics is to keep the gyros out of lockin. At very low input rates, the laser gyro scale factor degrades to zero, resulting in output error. So, some other kinematics must be used, which both keeps the gyro out of lockin and preserves computability. The standard way of doing this is to oscillate the gyro around its input axis, referred to as dithering the gyro. This avoids the computability problems of compound motion, exemplified by coning errors.

Dithering is conveniently done by mounting the gyro on a torsional spring (oriented around the input axis) and driving the gyro in an angular sinusoidal motion, typically a few hundred arc-sec peak-to-peak, at a frequency of a few hundred hertz.

Now, there is another problem. The dither oscillation goes to zero rate twice every dither cycle, and during these brief instants, lockin effects cause the gyro output to accrue small increments of error. Their rms value is a function of intrinsic gyro lockin rate and of the time spanning each dither reversal during which the angular dither rate is less than the lockin rate. Under ordinary randomized dither, the errors accumulate to a random walk angular output error. Typical dithered gyro random walks are 0.003, 0.001, and $0.00025^\circ/\text{rt-hr}$, for the GG1342, GG1300, and GG1389 Honeywell RLGs, respectively. As far as we know, the GG1389 has the lowest ordinary-dither random drift of any laser gyro in the world, but its value is still far too high to enable subarc-sec system performance.

Analytic modeling of the laser gyro has disclosed that the error increments incurred across each dither reversal are, other things being equal, sinusoidal functions of the nominal value of the gyro phase angle at the dither peak. Under randomized dither (in which the dither amplitude varies slightly for each successive dither peak), a random sequence of error increments is generated, which adds to a random walk. This model has been confirmed by many experiments.

Observed random drifts agree very well with this model (which is based on approximating the sinusoidal dither near the peak as a parabola, and then integrating the lockin equation to yield a pair of Fresnel integrals to represent the error increment). So, it was a natural step to pursue the model further and find ways to reduce the random drift. The CLIC invention was the result. This functions by controlling the dither in detail, in such a way that the trig functions (sine and cosine) of the gyro phase angle values at the

dither minimaxes sum to zero, rather than to an unbounded random walk. Then, with the trig functions held to zero sum, the drift error will likewise become bounded and low.

Upon implementing CLIC, gyro random drifts did decrease by a factor of up to tenfold. With some exceptions, it appears that CLIC makes the gyro perform up to the so-called quantum limit, as governed by the canonical uncertainty equations of quantum mechanics. Quantum-limited performance is also approached when the gyro is continuously rotated in one direction. This has been shown over five years of research and tests. The hoped-for value of $0.00004^\circ/\text{rt-hr}$ is about two times the calculated quantum limit. It seems reasonable to expect this value from a CLIC-enhanced GG1389, especially since it has been achieved under unidirectional rotation testing.

CLIC has a side benefit that is also vital to getting subarc-sec performance. It provides enhanced angular resolution, to within < 0.01 arc-sec, instead of the usual laser gyro pulse weight quantization (1 arc-sec, for the GG1389). This is done by the CLIC software for the original purpose of calculating gyro drift error discriminant values. Without this feature, each of the indexed readings taken would be corrupted by $1/\text{SQRT}(6)$ gyro pulses, i.e., 0.4 arc-sec rms. Even with only four readings per hour, this would generate added error of $0.00020^\circ/\text{rt-hr}$. This would result in performance of 5 times spec, instead of being almost in spec. But, with 0.01 arc-sec resolution, there would be negligible added effect.

CLIC has been well developed and refined over the last five years and needs no further development, beyond putting it into a different gyro than the presently-used GG1342. This entails some hardware additions to the gyro dither drive and readout, and simple changes in the software--mainly different values of constants for gyro scale factor, dither frequency, drive scale factor, etc.

SECTION 6

EXPERIMENTAL RESULTS

UNDITHERED GYRO RANDOM DRIFT CHARACTERISTICS

Having determined that a subarc-sec system would require random drifts of less than $0.000045^\circ/\text{rt-hr}$, we see that only the Honeywell GG1389 RLG could meet this goal, and then only when continuously rotated or, if dithered, only with CLIC. Since we don't have CLIC yet for the GG1389, we proceeded to concentrate on rate-biased tests. These were done by mounting the GG1389 on our Goertz Series 800 Direct-Drive Rate Table, with the input axis vertical, and rotating at 30 and $40^\circ/\text{sec}$.

The table has bounded-error in its angular measurement, of a nature that is readily dealt with by processing the output with a triangular filter. This drastically attenuates the bounded spillover/quantization error of the table readout, relative to the integrated white-noise angle random walk, and enables measurement of very low random walks that would otherwise be completely obscured by table bounded-error noise.

The original copious data stream obtained over 2° or 3° sectors of revolution was compacted while being generated into a much smaller number of triangular-filtered one-revolution data ensembles, which were stored in our Data General computer. They were subsequently computer-processed to generate variance plots, and best-fitted to a four-parameter curve, comprising residual bounded error, angle random walk, bias instability, and rate random walk, as defined by the values of the fitting coefficients.

The only thing that has delayed the application of CLIC in systems is that it depends on a computerized prediction of how the inertial rotation input to the gyro increments over one dither cycle (about 3 msec, for the GG1342). It needs to know this to within 0.2 arc-sec, in order to generate the right amount of modulation to change the next dither peak angle to a value that helps to keep the aforesaid sums of trig functions bounded. So, if there's noise in the angular environment of order 0.2 arc-sec uncorrelated over 3 msec, CLIC will break down. Because of this, CLIC is presently limited to benign environments, such as in the laboratory, on a rigid mounting.

The angular environment in the situation being discussed here is (or can easily be made so), an extremely benign one. This is a perfect application for CLIC. A CLIC-enhanced dithered laser gyro may be expected to give random drift performance equal to that of elaborately carouselled undithered laser gyros. Now, with no carouseling, one doesn't need three gyros to sort out the kinematics of compound rotations and to compute platform attitude. Rather, one gyro is rigidly attached in a well-defined relationship to the surface being measured. A one-gyro system may not be only equal to the three-axis system, but even better.

The results of this testing procedure are shown in Figures 10, 11 and 12. These comprise tests on GG1389 gyro no. 003, done on three different days, at 40°/sec with 3° sector data, and at 30°/sec with 2° sector data. In all these tests, the best fit is obtained with an angle random walk value of 0.000040°/rt-hr. We therefore infer this as the official value of undithered angle random walk for this gyro. This is close to meeting the requirements for the performance goal of 0.2 arc-sec rms measurement error over 16 hr, defined in Section 2, and is even lower than the value of 0.000045 assumed in Section 4 for the Dual-Freedom System Analysis and Simulation, using GG1389s.

INPUT AXIS STABILITY TESTS

Gyro input axis stability is as important a factor as random drift in a subarc-sec system, though of lesser relative importance in other kinds of application. For this reason, there had been little formal investigation of

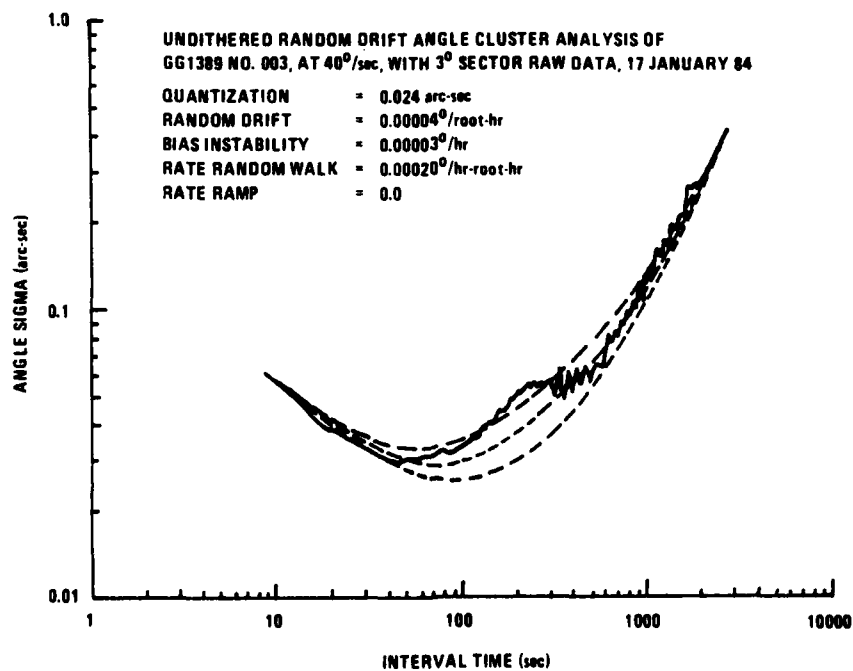


Figure 10. GG1389 Random Drift Analysis, 17 January 1984

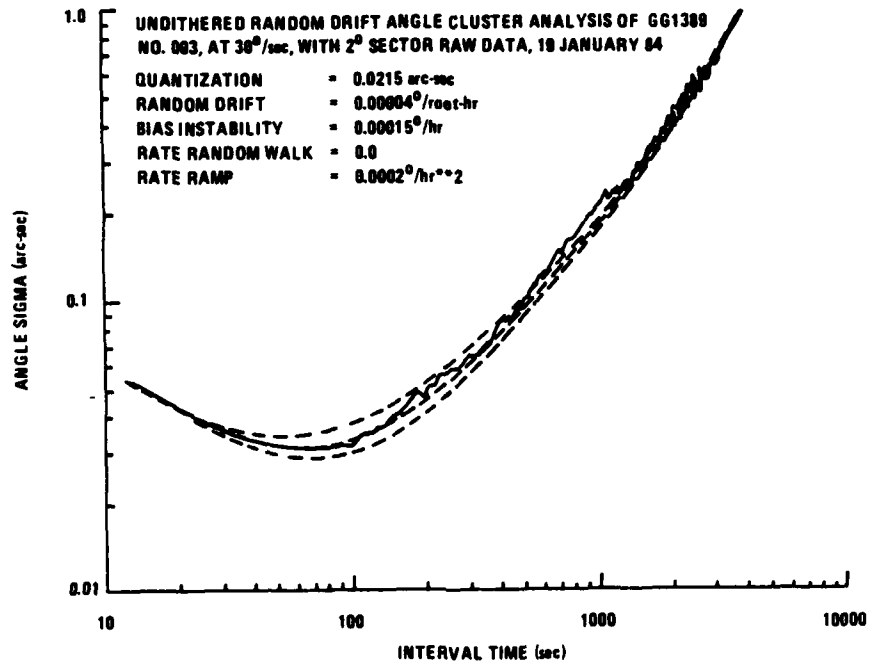


Figure 11. GG1389 Random Drift Analysis, 19 January 1984

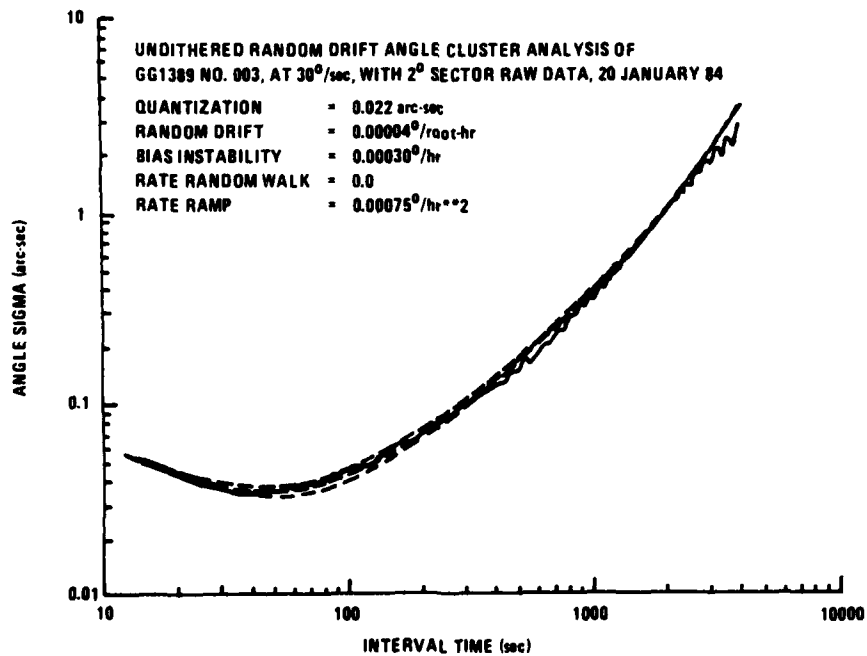


Figure 12. GG1389 Random Drift Analysis, 20 January 1984

laser gyro input axis stability. But recently, this situation has been remedied. We did a series of tests between March and May 1984 on three GG1389 laser gyros. These tests indicated a most gratifying degree of input axis stability, relative to the gyro block itself, with the worst component of the worst gyro being only ± 0.04 arc-sec. This is the intrinsic limiting stability. The input axis stability relative to the fixturing on which the gyros were mounted ranged from 0.25 to 0.90 arc-sec, from remount to remount. This emphasizes the need for carefully-made indexing fixtures for the one-axis subarc-sec demonstrator unit.

The experimental configuration was as follows: the gyro was mounted on a fixture with its input axis nominally in the horizontal plane. The fixture itself was mounted on the Goertz table, with the latter having rotation around a nominally vertical axis. The gyro was mounted on the fixture in four positions, indexed in 90° increments of rotation around the nominal gyro axis. The four positions are denoted NA up, NA down, LA up, and LA down. LA and NA denote two gyro body axes perpendicular to the nominal gyro axis (see Figures 13 and 14). The gyro was operated with dither on, and with angular input generated by rotating the Goertz table through many revolutions, both clockwise and counterclockwise.

Nominally, with the gyro axis perfectly orthogonal to the Goertz table rotation axis, the only gyro output will be gyro bias and random walk, plus a small contribution due to earth rate, seen as a sinusoidal signal, at the frequency of rotation of the Goertz table, with an amplitude equal to horizontal-plane earth rate (earth rate times cosine of latitude). But, with data taken over an integral number of Goertz table rotations, the latter sums to zero. (This assumes a constant rate of rotation of the Goertz table, which is almost exactly the case.)

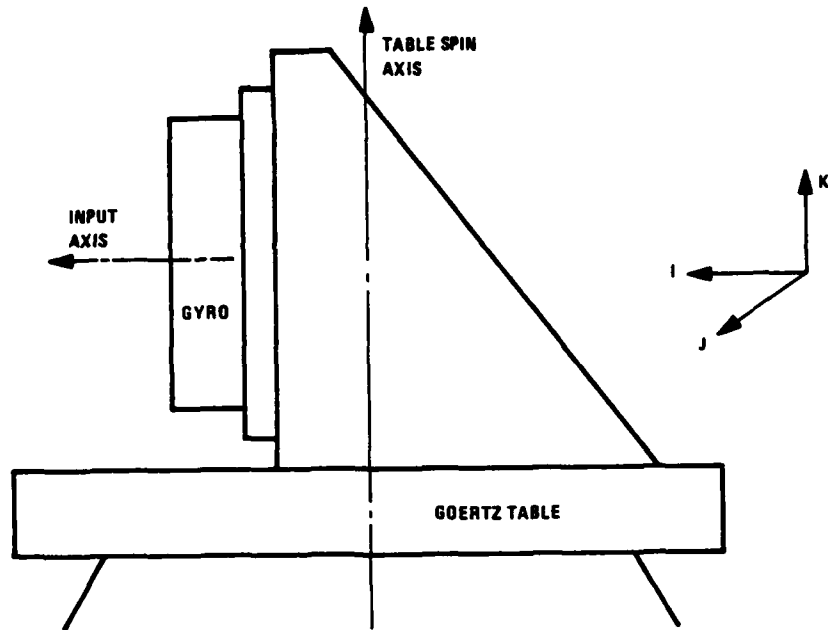


Figure 13. Input Axis Stability Test Set-Up, Side View

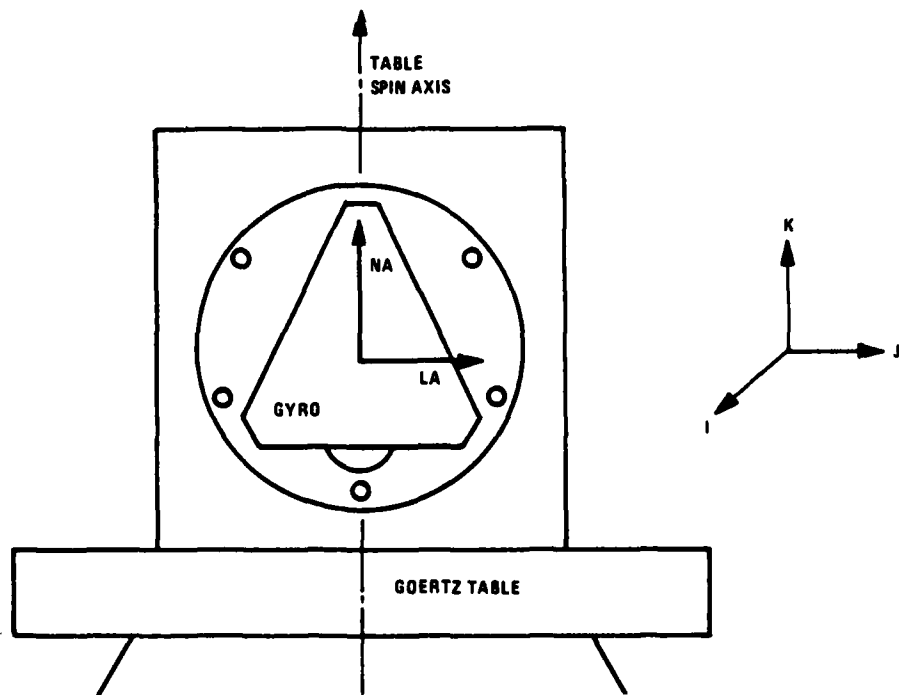


Figure 14. Input Axis Stability Test Set-Up, Front View

So, the output will comprise bias, plus random drift, plus a contribution due to the gyro axis unit vector having a small component along the Goertz table rotation axis unit vector. Using small angle approximations, the resulting output per Goertz table revolution will equal the gyro scale factor, in counts/revolution, times the component of the gyro axis along the Goertz axis, times an adjustment for the earth rate component along the Goertz axis.

From the results of the eight runs, we can determine gyro bias, two components of non-orthogonality of the gyro sensing axis to the LA-NA plane, and non-orthogonality between the normal to the LA-NA plane and the Goertz table rotation axis. With this factor-of-two overdeterminacy, we can also form estimates of the stability of the above four variables. The computations are based on the following model of gyro input axis deviation.

Gyro axis unit vector, V , = I + perturbation, D . The values of D in the 4 gyro orientations are

$$D(\text{NAU}) = J*GL+K*(MK+GN)$$

$$D(\text{NAD}) = -J*GL+K*(MK-GN)$$

$$D(\text{LAU}) = -J*GN+K*(MK+GL)$$

$$D(\text{LAD}) = J*GN+K*(MK-GL)$$

where:

I = nominal V , perpendicular to K

J = in-plane axis, perpendicular to I and K

K = Goertz rotation axis

GL = Component of D along LA body axis

GN = Component of D along NA body axis

MK = Component of tilt of indexing axis along K

The one-revolution output that would be seen along the Goertz axis at rate R is

$$CR = SF*(EV+R)/|R|$$

where:

SF = Gyro scale factor, in counts/revolution

EV = Component of earth rate along the Goertz axis

R = Rate of rotation around Goertz axis

The gyro output over one revolution will equal CR times the component of V along the Goertz axis, plus gyro bias rate times the period of revolution times scale factor:

$$GY = SF*BG*TAU/2*PI + DK*CR$$

where:

GY = One-rev gyro output, in counts

BG = Bias rate of gyro, in radians per second

TAU = Period of revolution around Goertz axis, in seconds

DK = Component of D along Goertz axis

PI = 3.1415937022.....

The foregoing is applied as follows: the method will be exemplified by working out the set of stability values for GG1389 gyro no. 011, using the measurements taken for that gyro.

Equating the expressions for the eight outputs to the values actually measured, we get the following eight equations.

$$\begin{aligned}
\text{GY(NAU, CCW)} &= \text{BT} + \text{SF} \cdot (1 + \text{EPS}) \cdot (\text{MK} + \text{GN}) = 110.159 \text{ counts} & (6-1) \\
\text{GY(NAU, CW)} &= \text{BT} - \text{SF} \cdot (1 - \text{EPS}) \cdot (\text{MK} + \text{GN}) = -110.600 \text{ counts} & (6-2) \\
\text{GY(NAD, CCW)} &= \text{BT} + \text{SF} \cdot (1 + \text{EPS}) \cdot (\text{MK} - \text{GN}) = -19.560 \text{ counts} & (6-3) \\
\text{GY(NAD, CW)} &= \text{BT} - \text{SF} \cdot (1 - \text{EPS}) \cdot (\text{MK} - \text{GN}) = 20.080 \text{ counts} & (6-4) \\
\text{GY(LAU, CCW)} &= \text{BT} + \text{SF} \cdot (1 + \text{EPS}) \cdot (\text{MK} + \text{GL}) = 33.980 \text{ counts} & (6-5) \\
\text{GY(LAU, CW)} &= \text{BT} - \text{SF} \cdot (1 - \text{EPS}) \cdot (\text{MK} + \text{GL}) = -33.580 \text{ counts} & (6-6) \\
\text{GY(LAD, CCW)} &= \text{BT} + \text{SF} \cdot (1 + \text{EPS}) \cdot (\text{MK} - \text{GL}) = 82.220 \text{ counts} & (6-7) \\
\text{GY(LAD, CW)} &= \text{BT} - \text{SF} \cdot (1 - \text{EPS}) \cdot (\text{MK} - \text{GL}) = -81.700 \text{ counts} & (6-8)
\end{aligned}$$

where:

$$\begin{aligned}
\text{BT} &= \text{SF} \cdot \text{BG} \cdot \text{TAU} / 2 \cdot \text{PI} \\
\text{EPS} &= \text{EV} / |\text{R}|
\end{aligned}$$

Using Equations 6-1 and 6-3:

$$\text{BT} + \text{SF} \cdot (1 + \text{EPS}) \cdot \text{MK} = (110.159 - 19.560) / 2 = 45.2995 \text{ counts}$$

Using Equations 6-2 and 6-4:

$$\text{BT} - \text{SF} \cdot (1 - \text{EPS}) \cdot \text{MK} = -45.2600 \text{ counts}$$

whereby

$$\text{MK} = 45.2798 / \text{SF}$$

and

$$\text{BT} = 0.0198 - 45.2798 \cdot \text{EPS}$$

On the other hand, we have

Equations 6-5 and 6-7

$$BT + SF \cdot (1 + EPS) \cdot MK = 58.1000 \text{ counts}$$

Equations 6-6 and 6-8

$$BT - SF \cdot (1 - EPS) \cdot MK = -57.6400 \text{ counts}$$

whereby:

$$MK = 57.8700 / SF$$

and

$$BT = 0.2300 - 57.8700 \cdot EPS$$

Values of the constants are

$$SF = 1296000 \text{ counts/revolution}$$

$$R = 30^\circ/\text{sec}$$

$$EV = 10.63564^\circ/\text{hr at latitude } 45^\circ \text{ north}$$

$$\text{Hence, } EPS = 10.63564 / (30 \cdot 3600) = 0.00009848$$

Therefore:

$$MK(1234) = 45.2798 / 1296000 \text{ rad} = 7.20 \text{ arc-sec}$$

$$MK(5678) = 57.8700 / 1296000 \text{ rad} = 8.10 \text{ arc-sec}$$

i.e., $MK = 7.65 \pm 0.45$ arc-sec.

$$BT(1234) = 0.0153 * 180 * 3600 / 1296000 * \pi = 0.0024 \text{ arc-sec}$$

$$BT(5678) = 0.2300 * 180 * 3600 / 1296000 * \pi = 0.0370 \text{ arc-sec}$$

i.e., $BT = 0.020 \pm 0.017$ arc-sec.

Furthermore, subtracting Equation 6-3 from Equation 6-1,

$$GN(13) = 64.859 / (SF * (1 + EPS)) = 10.322 \text{ arc-sec}$$

and subtracting Equation 6-4 from Equation 6-2,

$$GN(24) = 65.320 / (SF * (1 - EPS)) = 10.397 \text{ arc-sec}$$

i.e., $GN = 10.360 \pm 0.037$ arc-sec.

Similarly, subtracting Equation 6-7 from 6-5,

$$GL(57) = -24.12 / (SF * (1 + EPS)) = -3.838 \text{ arc-sec}$$

and, subtracting Equation 6-8 from 6-6,

$$GL(68) = -24.06 / (SF * (1 - EPS)) = -3.830 \text{ arc-sec}$$

i.e., $GL = -3.834 \pm 0.004$ arc-sec

The results for no. 011 are summarized in Table 2.

TABLE 2. SHORT-TERM AXIS STABILITIES OF GG1389 NO. 011

Term	Value in Arc-Sec	Variation in Arc-Sec
MK	7.65	± 0.45
BT	0.020	± 0.017
GN	10.360	± 0.037
GL	-3.834	± 0.004

We saw a qualitative repeat of these results on numbers 009 and 004. That is, very low variability in three terms, and relatively high variability in the tilt of the fixture indexing axis, MK. This further strengthens the conjecture that there is either aniso-sag of the gyro dither post under the cantilevered weight load of the gyro (as between the set of NA up and down measurements and the set of LA up and down measurements), or else aniso-flexure of the gyro base plate, or even (less plausibly) aperture-connected bias shift due to aniso-sag effects on the gyro mirrors, and hence on the location of the laser beam path triangle.

After the above tests, a series of tests were run over a three-day period, comprising CCW and CW runs in the LA down orientation only. The results are presented in Table 3.

TABLE 3. MULTIDAY DATA OF GG1389 NO. 011

	CCW	CW	Sum/2	Diff/4*PI
Day 1	90.819	-89.920	0.450	14.38
Day 2	92.400	-91.401	0.500	14.63
Day 3	92.440	-91.520	0.460	14.64

The daily readings, when differenced, yield the sets of day-to-day differences listed in Table 4.

TABLE 4. MULTIDAY STABILITIES OF GG1389 NO. 011

	Delta-Sum/2	Delta-Diff/4*PI
Day 2 - Day 1:	0.05	0.15
Day 3 - Day 2:	-0.04	0.01

Diff/4*PI represents the value of MK-GL, while Sum/2 represents BT. The above data suggests that both MK (to do with aniso-sag, etc.), and the gyro intrinsic bias were rather stable over a three-day period, more so than was seen in gyros 1-009 and 1-004.

The counts/rev data for GG1389 gyro no. 009 are listed in Table 5.

TABLE 5. MULTI-ORIENTATION DATA FOR GG1389 NO. 009

NA up CCW	316.329
NA up CW	-317.700
NA down CCW	298.698
NA down CW	-300.060
LA up CCW	254.500
LA up CW	-255.779
LA down CCW	366.423
LA down CW	-367.962

From these data, we computed the set of stabilities listed in Table 6.

TABLE 6. SHORT-TERM AXIS STABILITIES OF GG1389 NO. 009

Term	Value in Arc-Sec	Variation in Arc-Sec
MK	49.3	± 0.25
BT	-1.018	± 0.007
GN	1.400	± 0.005
GL	-8.92	± 0.02

Then, multiday stability data were taken, as presented in Table 7.

TABLE 7. MULTIDAY DATA OF GG1389 NO. 009

	CCW	CW	Sum/2	Diff/4*PI
Day 1	366.423	-367.962	-0.77	58.44
Day 3	364.621	-366.379	-0.88	58.17
Day 6	378.859	-380.403	-0.77	60.42
Day 7	378.561	-380.282	-0.86	60.39

Plausibly, the multiday variation of ± 0.05 arc-sec in the half sum suggests a bias instability of order $0.00008^\circ/\text{hr}$. The small changes in the differences between Days 1 and 3 and between days 6 and 7 (0.27 and 0.03 arc-sec, respectively) are compatible with the one-day data stabilities listed in Table 6. The 2.2 arc-sec jump between Days 3 and 6 may be due to some shift in

the mounting hardware, associated with shutting down for the weekend. The GG1389 no. 004 was also tested, giving the one-rev data listed in Table 8.

TABLE 8. MULTI-ORIENTATION DATA FOR GG1389 NO. 004

NA	up	CCW	35.280
NA	up	CW	-36.000
NA	down	CCW	198.740
NA	down	CW	-199.921
LA	up	CCW	20.120
LA	up	CW	-21.420
LA	down	CCW	236.979
LA	down	CW	-237.980

The multiday data obtained are presented in Table 9.

TABLE 9. MULTIDAY DATA OF GG1389 NO. 004

	CCW	CW	Sum/2	Diff/4*PI
Day 1	240.040	-241.021	-0.490	38.28
Day 2	237.501	-238.478	-0.488	37.88
Day 3	234.681	-236.039	-0.679	37.46

From the data in Tables 8 and 9, we infer the stabilities for GG1389 no. 004 that are listed in Tables 10 and 11.

TABLE 10. SHORT-TERM AXIS STABILITIES OF GG1389 NO. 004

Term	Value in Arc-Sec	Variation in Arc-Sec
MK	7.65	± 0.45
BT	0.020	± 0.017
GN	10.360	± 0.037
GL	-3.834	± 0.004

TABLE 11. MULTIDAY STABILITIES OF GG1389 NO. 004

	Delta (Sum/2)	Delta (Diff/4*PI)
Day 2 - Day 1	0.002	-0.40
Day 3 - Day 2	-0.190	-0.42

TILTMETER CHARACTERISTICS

Since, in a one-axis system, the two tiltmeters could do '2/3 of the job' (tilt around north and east), it is fitting to discuss tiltmeter characteristics. Figure 15 shows (inferentially) the stability of the simple bubble-level tiltmeter, as it existed in 1963, over a one-year period. Two bubble levels were placed along east-west and along north-south, for a total of four. For clarity, the vertical scales were staggered, so that each of the four outputs could be clearly seen. The two pairs track each other very well. Apart from some exceptional periods (notably, around June for the east-west pair) they seem to track within a fraction of an arc-sec, perhaps within 0.1 arc-sec. Whoever prepared this graph would have been a hero had he/she thought to plot the differences between the tiltmeter pairs! Unfortunately, the data records are long gone.

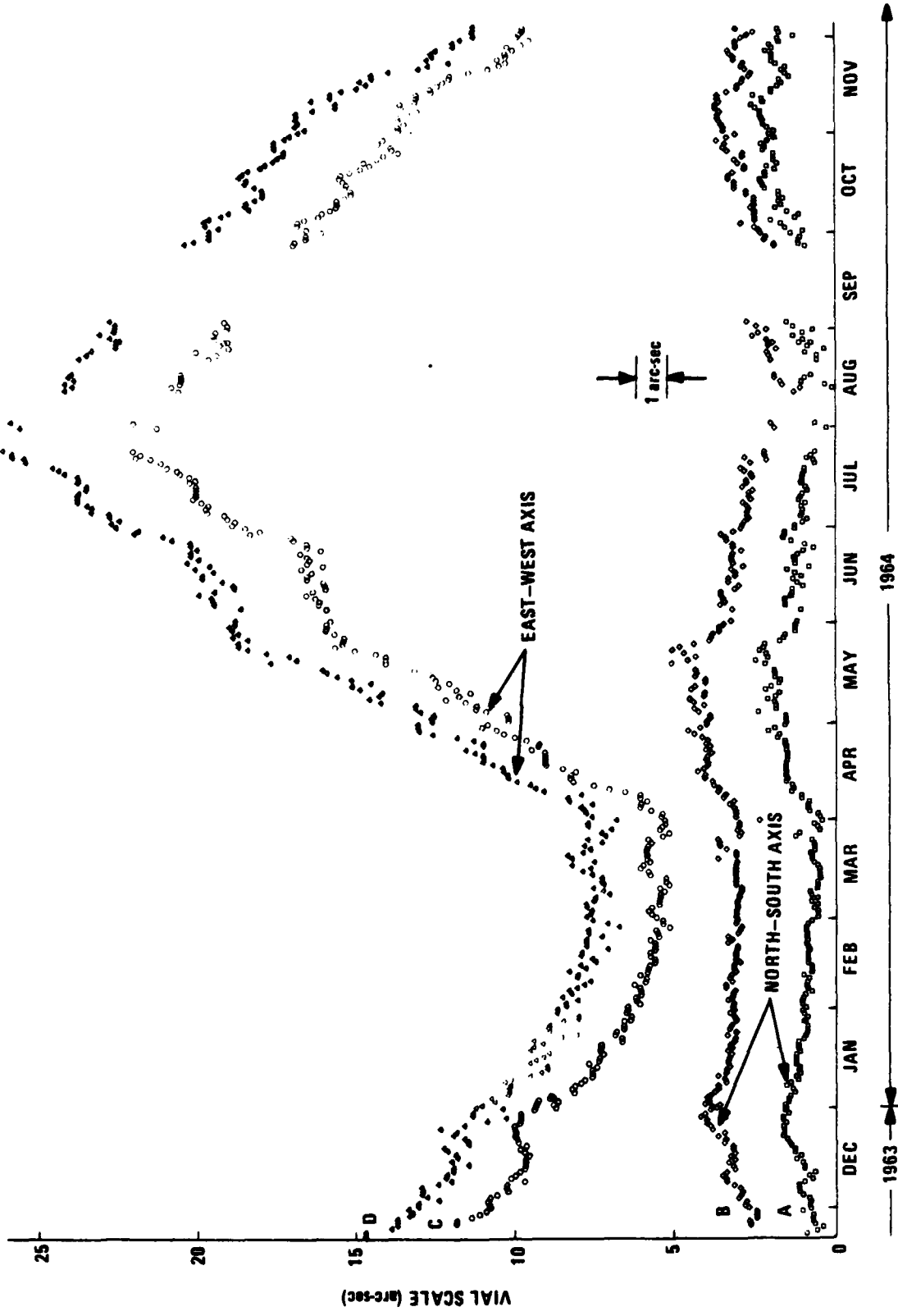


Figure 15. Stability of Bubble Tiltmeter (over 12 months)

These were 1963 state-of-the-art bubble tiltmeters. There have been many refinements since then, notably in the area of digitized readout mechanizations, with accuracies quoted at 0.05 arc-sec rms. Thus, it is reasonable to assume that tiltmeter errors will RSS negligibly with gyro errors.

SECTION 7

CONCLUSIONS AND RECOMMENDATIONS

CONCLUSIONS

1. It looks marginally feasible to measure crustal rotation around the vertical to an accuracy of 0.2 arc-sec rms, over a period of 16 hr, using either a three-axis navigator-type system, comprising three GG1389 laser gyros, plus three accelerometers with special two-degree of freedom carouseling; or a one-axis system, comprising one dithered CLIC-enhanced GG1389 laser gyro, indexed between east and west, plus two tiltmeters.
2. It is impracticable to distinguish between crustal rotation displacement around the vertical and EPA deviation along east-west using self-contained measurements from a single apparatus at one site. Either a central station determination of earth spin axis deviation must be made and applied to the total apparatus reading, or possibly multisite averaging may be used.
3. The vertical axis component of the three-axis system angle sensing is relatively useless, because it is random-walk-driven without any possibility of correction from accelerometer 'tilt' readings. Its error is bounded only by conflicting rate information generated along the east axis.
4. The two tilt components of earth crustal rotation (around north and east) can be readily and adequately measured by two tiltmeters. Gyros are needed only to add information around the vertical.
5. The best deployment of gyro power is along east-west.

6. The one-axis system would probably work at least as well as the three-axis system, assuming that accurate indexing can be done.

RECOMMENDATIONS

Based on the results of this study and on our perceptions of AFGL's needs, we recommend that AFGL initiate a program to design, build, and test a transportable one-axis demonstrator. As well as showing (or disproving) feasibility, the demonstrator prototype will indicate further areas to be studied, refinements needed in the kinematics, added error sources, etc. It will be the first transportable subarc-second crustal deviation measurement device to be built, so all the data it generates will be of the utmost interest in guiding future development.

Recommended Demonstrator Design

The proposed demonstrator is a single-axis indexed system with two tiltmeters and a single GG1389 RLG. The sensors and their electronics are fixed to a platform that is mounted on a computer-driven ULTRADEX precision indexing table. The outputs of all of the sensors will be continuously monitored via a dedicated processor that will perform the algorithm calculation and output the results to a graphics display, thus allowing continuous monitoring of the performance of the system.

A block diagram of the demonstrator hardware is shown in Figure 16. The laser gyro is mounted with its input axis nominally horizontal, in the plane of the plate surface, along a direction that will be nominally east-west when installed. Two tiltmeters are mounted to sense tilts around nominal east-west, and around nominal north-south. A block schematic of the electronics is given in Figure 17.

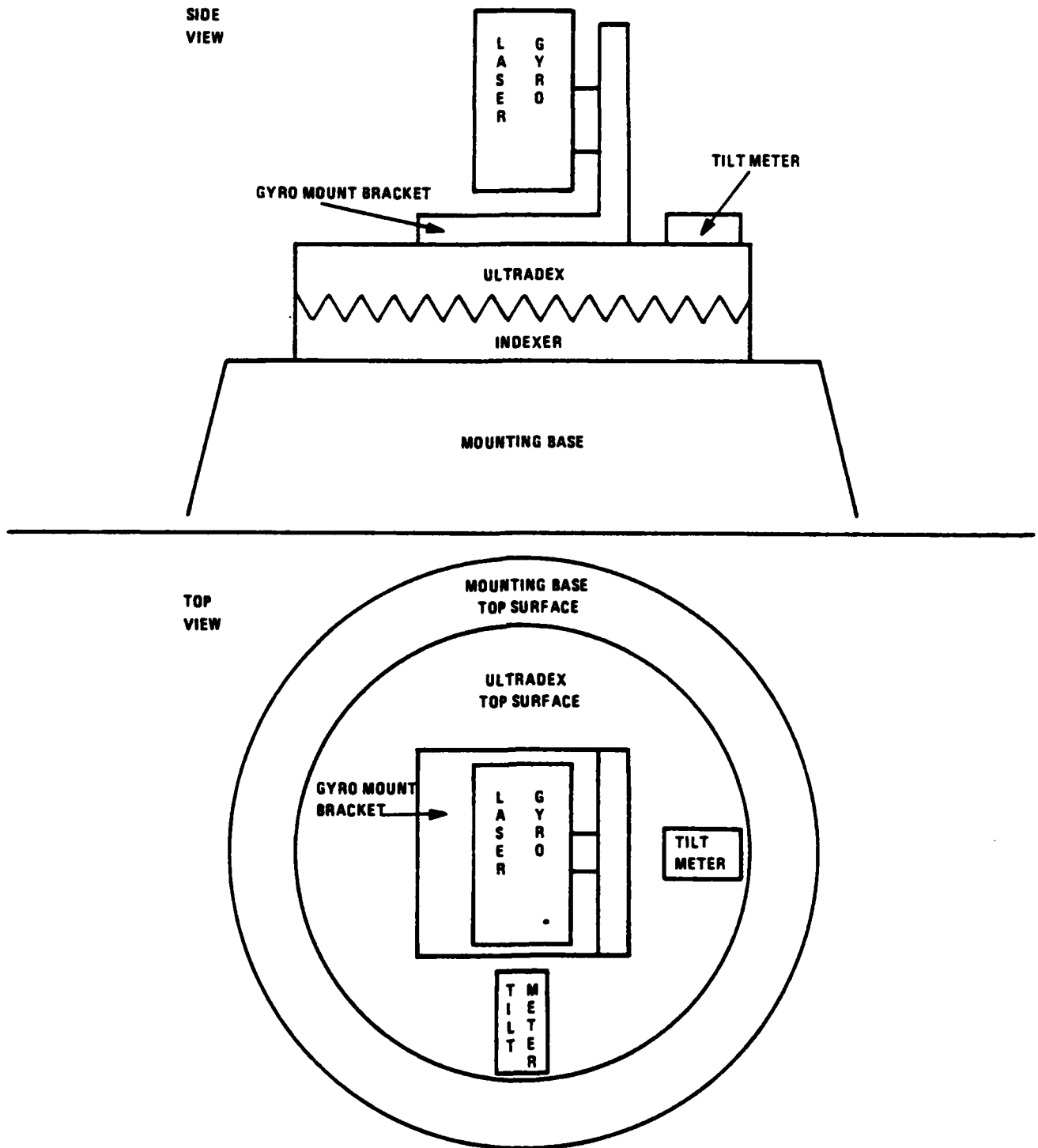


Figure 16. Block Diagram of Proposed Demonstrator Hardware

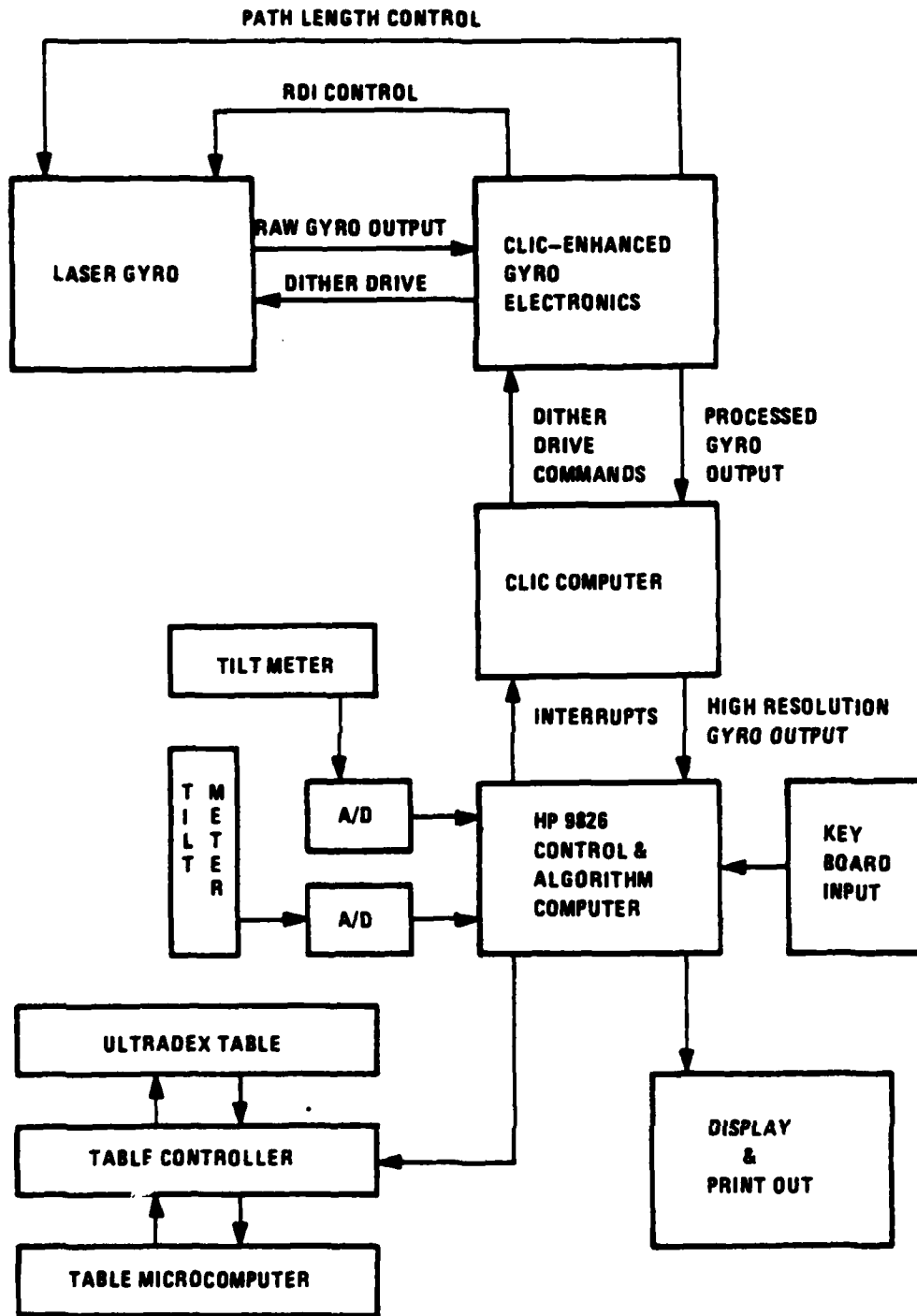


Figure 17. Block Schematic of Demonstrator Electronics

The ULTRADEX indexing table is the platform to which all the sensors and their electronics are fixed. This table is computer-precision controlled, with position error of $< 1/8$ arc-sec, and repeatability better than $1/20$ arc-sec, around the index axis. The rotation axis instability is nominally 1 to 2 arc-sec random. This latter component is attenuated over N successive indexes, by a factor of $\text{SQRT}(N)$. If this instability becomes a concern, it would be possible to measure the relative tilt angle between the top and bottom surfaces of the platform and explicitly eliminate the effect of rotation axis instability. This would entail using added high-stability tiltmeters. The present system design does not include extra tiltmeters, but has expansion capability to add them at a later date. In addition, the system will allow changing to different RLGs with minimal modification, thereby facilitating system performance upgrades as technology produces even better RLGs.

The computation algorithm will be fed by the outputs of the sensors, and its cycle will extend over each period between successive indexations. The results of successive cycles will be appropriately filtered to yield a progressively improved estimate of 1) crustal tilt around some horizontal plane axis, and 2) combined east-west deviation of the polar axis and crustal rotation around the vertical. The control and algorithm processor planned for use is the Hewlett-Packard HP9826. This machine has been chosen for its interface capability to physical sensors and for its straightforward high-order language operating system. These factors will allow the control and algorithm software to be written in a concise and efficient manner.

Demonstrator Features

Automated Operation--Fully automatic data acquisition and control, allowing unattended operation for extended periods of time.

On-Line Calculation--Real-time calculation of combined polar axis deviation and earth crustal rotation around the vertical, from the initial-condition state.

Portability--Rugged design, combined with reasonable size and weight, to allow easy transport to other laboratory sites for test and demonstration.

Reliability--RLG life and reliability have been clearly demonstrated in commercial aircraft revenue service, with MTBF in excess of 50000 hr.

APPENDIX A

ANALYSIS OF DUAL-FREEDOM ROTATIONAL STRATEGY

APPENDIX A

ANALYSIS OF DUAL-FREEDOM ROTATIONAL STRATEGY

ERROR MODEL

The following error model is assumed.

$$\dot{\underline{\Psi}} = -C_g \delta\omega \quad (A-1)$$

$$\dot{\delta\underline{V}} = C_a \delta\underline{a} - \underline{\Psi} \underline{x}_a \quad (A-2)$$

where:

- $\underline{\Psi}$ = attitude error vector of orthogonal ISA system axes relative to an earth-fixed frame
- $\delta\underline{V}$ = velocity error vector
- \underline{a} = nongravitation acceleration vector of ISA
- C_g = transformation matrix from gyro input axes to local-vertical reference frame
- C_a = transformation matrix from orthogonal accelerometer input axes to local-vertical reference frame
- $\delta\omega$ = gyro output error vector
- $\delta\underline{a}$ = accelerometer output error vector

The question is, how must the sensor assembly be rotated to cause attitude and velocity error to have a mean value of zero.

The matrix C_g can be expressed as the product of the matrix A (which relates the gyro input axes to the system frame), and the matrix C (which relates the ISA frame to the local-vertical reference axes).

$$C_g = CA \quad (A-3)$$

The total error in the gyro output ($\delta\omega$) can be decomposed in terms of bias, scale factor, and misalignment errors as

$$\delta\omega = \delta A^{-1} \omega_{r/i} + K_g \omega_{g/i} + \underline{b}_g \quad (A-4)$$

where:

$\omega_{r/i}$ = inertial angular velocity of the ISA

$\omega_{g/i}$ = inertial angular velocity measured by the gyro triad

\underline{b}_g = gyro bias error

δA^{-1} = error in transformation matrix from ISA axes to gyro axes

K_g = gyro scale factor error matrix

Putting Equations A-3 and A-4 into Equation A-1 yields:

$$\begin{aligned} \dot{\Psi} &= CA(\delta A^{-1} \omega_{r/i} + K_g \omega_{g/i} + \underline{b}_g) \\ &= CA(\delta A^{-1} \omega_{r/i} + K_g A^{-1} \omega_{r/i} + \underline{b}_g) \\ &= CA[(\delta A^{-1} + K_g A^{-1}) \omega_{r/i} + \underline{b}_g] \end{aligned} \quad (A-5)$$

The effect of gyro input axis misalignment on A^{-1} can be expressed as

$$\delta A^{-1} = \sum_{i=1}^m \frac{\partial A^{-1}}{\partial \delta_i} \delta_i \quad (A-6)$$

where the δ_i 's are the gyro misalignment angles. The gyro scale factor error matrix, K_g , can also be explicitly defined as

$$K_g = \text{diag} (k_{g1} \ k_{g2} \ k_{g3}) \quad (A-7)$$

where the k_{g_i} 's are the gyro scale factor errors and "diag" denotes a diagonal matrix. Substituting Equations A-6 and A-7 into Equation A-5 gives:

$$\dot{\underline{\Psi}} = CA \left[\left(\sum_{i=1}^m \frac{\partial A^{-1}}{\partial \delta_i} \delta_i + \text{diag} (k_{g1} \ k_{g2} \ k_{g3}) A^{-1} \right) \underline{\omega}_{r/i} + \underline{b}_g \right] \quad (\text{A-8})$$

The accelerometer output error is expressed as

$$\delta \underline{a} = K_a \underline{a} + \underline{b}_a \quad (\text{A-9})$$

where:

\underline{a} = nongravitational acceleration expressed with components in the system frame

\underline{b}_a = accelerometer bias

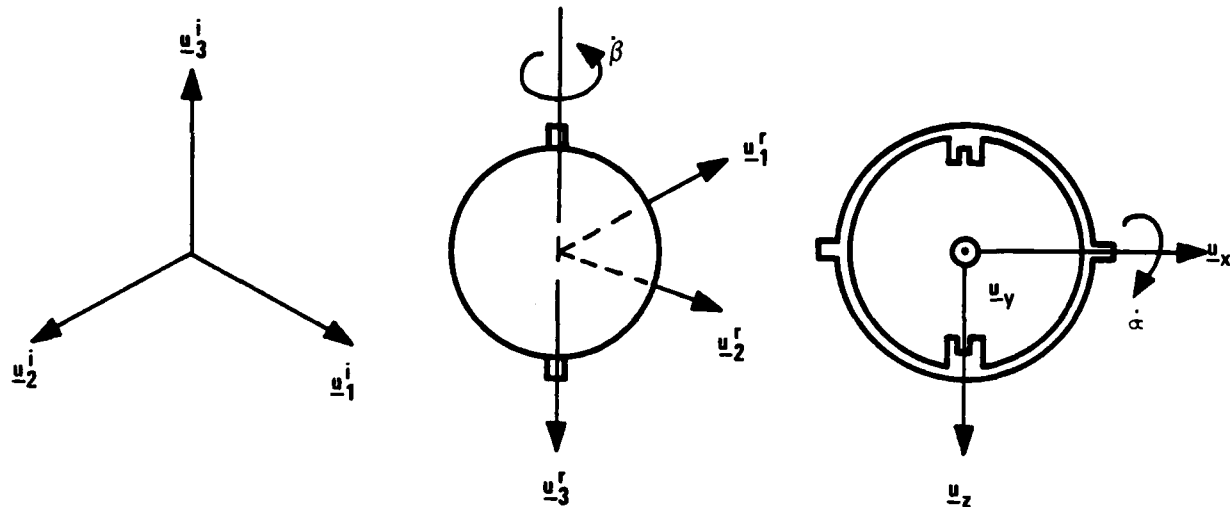
and K_a is a matrix that accounts for both misalignment and scale factor error (the diagonal entries being scale factor errors and the off-diagonal entries being misalignment errors). Since the accelerometer input axes nominally coincide with the ISA system axes, the matrix C_a in Equation A-2 can be replaced by C , which allows Equation A-2 to be written as

$$\delta \dot{\underline{V}} = C[K_a \underline{a} + \underline{b}_a] - \underline{\Psi} \times \underline{a} \quad (\text{A-10})$$

CONDITIONS FOR COMMUTATION OF GYRO ERRORS

Referring to Figure A-1, we see that the angular rotation vector of the ISA can be expressed as

$$\underline{\omega}_{r/i} = \dot{\alpha} \underline{u}_x - \dot{\beta} \underline{u}_3^r \quad (\text{A-11})$$



a. Inertial frame b. ISA reference frame c. Outer gimbal reference frame

Figure A-1. Definition of Coordinate Frames

where:

$\dot{\alpha}$ = outer gimbal inertial rotation rate

$\dot{\beta}$ = inner gimbal inertial rotation rate

and the inertial rotational rate about the axis perpendicular to the two gimbal axes is taken to be zero. The unit vector \underline{u}_x belongs to the triad $(\underline{u}_x, \underline{u}_y, \underline{u}_z)$ attached to the outer gimbal, and \underline{u}_3^r belongs to the triad $(\underline{u}_1^r, \underline{u}_2^r, \underline{u}_3^r)$ that defines the ISA axes. If these two triads are assumed coincident at $t=0$, the subsequent transformation between them is defined by:

$$\begin{bmatrix} \underline{u}_x \\ \underline{u}_y \\ \underline{u}_z \end{bmatrix} = \begin{bmatrix} C\beta & S\beta & 0 \\ -S\beta & C\beta & 0 \\ 0 & 0 & 1 \end{bmatrix} \begin{bmatrix} \underline{u}_1^r \\ \underline{u}_2^r \\ \underline{u}_3^r \end{bmatrix} \quad (\text{A-12})$$

which allows the ISA rotation rate to be expressed as

$$\dot{\underline{\omega}}_{r/i} = \dot{\alpha}C\beta\underline{u}_1^r + \dot{\alpha}S\beta\underline{u}_2^r - \dot{\beta}\underline{u}_3^r \quad (\text{A-13})$$

If the inertial reference triad ($\underline{u}_1^i, \underline{u}_2^i, \underline{u}_3^i$) is also taken as being coincident with the other two triads at $t=0$, the following is true.

$$\begin{bmatrix} \underline{u}_1^i \\ \underline{u}_2^i \\ \underline{u}_3^i \end{bmatrix} = \begin{bmatrix} 1 & 0 & 0 \\ 0 & C\alpha & -S\alpha \\ 0 & S\alpha & C\alpha \end{bmatrix} \begin{bmatrix} \underline{u}_x \\ \underline{u}_y \\ \underline{u}_z \end{bmatrix}$$

Which, with Equation A-12, leads to the defining relationship for C:

$$\begin{bmatrix} \underline{u}_1^i \\ \underline{u}_2^i \\ \underline{u}_3^i \end{bmatrix} = \begin{bmatrix} C\beta & S\beta & 0 \\ -C\alpha S\beta & C\alpha C\beta & -S\alpha \\ -S\alpha S\beta & S\alpha C\beta & C\alpha \end{bmatrix} \begin{bmatrix} \underline{u}_1^r \\ \underline{u}_2^r \\ \underline{u}_3^r \end{bmatrix} = C \begin{bmatrix} \underline{u}_1^r \\ \underline{u}_2^r \\ \underline{u}_3^r \end{bmatrix} \quad (\text{A-14})$$

Using Equations A-13 and A-14 the attitude error propagation equation (A-8), can be expressed as

$$\dot{\underline{\Psi}} = \underline{\Pi} \underline{\epsilon}_g \quad (\text{A-15})$$

where $\underline{\varepsilon}_g$ is the gyro error vector:

$$\underline{\varepsilon}_g = (\delta_1 \delta_2 \dots \delta_m \quad k_{g_1} \quad k_{g_2} \quad k_{g_3} \quad b_{g_1} \quad b_{g_2} \quad b_{g_3})^T \quad (A-16)$$

and the elements of the matrix H are given by:

$$h_{ij} = \sum_{k=1}^m a_k f_k(t) \quad (A-17)$$

in which $f_k(t)$ is the k th of M time-dependent functions, and the a_k 's are constants that are functions only of the elements of the transformation matrix A.

If all sensor errors are assumed constant over time T, then Equation A-15 can be directly integrated:

$$\underline{\Psi}(T) = \left[\int_0^T H(t) dt \right] \underline{\varepsilon}_g \quad (A-18)$$

Furthermore, for $\underline{\Psi}(T)$ to equal zero:

$$\int_0^T f_k(t) dt = 0 \quad k = 1, 2, \dots, M \quad (A-19)$$

The integrals of the $f_k(t)$ that appear in the solution of the attitude error vector $\underline{\Psi}$ are defined in Table A-1, which shows that all of the functions to be integrated depend only on the gimbal angles and rates. If the ISA inertial rotation rates about the two gimbal axes are constant, all of the integrals can be evaluated explicitly. As an example, one of the Table A-1 integrals is evaluated as follows.

TABLE A-1. INTEGRAL FUNCTIONS FOR ATTITUDE ERROR PROPAGATION

	$\int f_k(t)dt$	Acceptable Ratio of Gimbal Rates*
Originating from Gyro Bias Errors	$\int \cos \delta t$	All n
	$\int \sin \delta t$	All n
	$\int \sin \alpha t$	All n
	$\int \cos \alpha t$	All n
	$\int \sin \alpha \sin \delta t$	n ≠ 1
	$\int \cos \alpha \sin \delta t$	All n
	$\int \sin \alpha \cos \delta t$	All n
	$\int \cos \alpha \cos \delta t$	n ≠ 1
Originating from Gyro Scale Factor and Misalignment Errors	$\int \dot{\alpha} \sin 2\delta t$	All n
	$\int \dot{\alpha} \sin \alpha \sin \delta t$	n ≠ 1
	$\int \dot{\alpha} \cos \alpha \sin \delta t$	All n
	$\int \dot{\alpha} \sin \alpha \cos \delta t$	All n
	$\int \dot{\alpha} \cos \alpha \cos \delta t$	All n
	$\int \dot{\alpha} \sin^2 \delta t$	No n
	$\int \dot{\alpha} \cos^2 \delta t$	No n
	$\int \dot{\alpha} \sin \alpha \sin^2 \delta t$	All n
	$\int \dot{\alpha} \cos \alpha \sin^2 \delta t$	All n
	$\int \dot{\alpha} \sin \alpha \cos^2 \delta t$	All n
	$\int \dot{\alpha} \cos \alpha \cos^2 \delta t$	All n
	$\int \dot{\alpha} \sin \alpha \sin 2\delta t$	All n
	$\int \dot{\alpha} \cos \alpha \sin 2\delta t$	All n

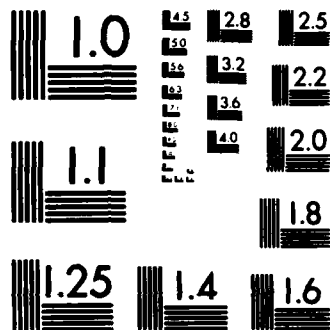
* The ratio (n) of inner to outer gimbal rates that produces a zero value of the integral over the period of the outer gimbal motion

TABLE A-1. INTEGRAL FUNCTIONS FOR ATTITUDE ERROR PROPAGATION (concluded)

	$\int f_k dt$	Acceptable Ratio of Gimbal Rates
Originating from Gyro Scale Factor and Misalignment Errors	$\int \dot{\beta} \cos \delta dt$	All n
	$\int \dot{\beta} \sin \delta dt$	All n
	$\int \dot{\beta} \sin \alpha dt$	All n
	$\int \dot{\beta} \cos \alpha dt$	All n
	$\int \dot{\beta} \sin \alpha \sin \delta dt$	$n \neq 1$
	$\int \dot{\beta} \cos \alpha \sin \delta dt$	All n
	$\int \dot{\beta} \sin \alpha \cos \delta dt$	All n
	$\int \dot{\beta} \cos \alpha \cos \delta dt$	$n \neq 1$

$$\begin{aligned}
 \int_0^T \dot{\alpha} \cos \alpha \sin^2 \beta dt &= \dot{\alpha} \int_0^T \cos \alpha t \sin^2 \beta t dt \\
 &= \frac{\dot{\alpha}}{2} \left[\int_0^T \cos \alpha t dt - \int_0^T \cos \alpha t \cos 2\beta t dt \right] \\
 &= \frac{1}{2} \left[\sin \alpha t \right]_0^T \\
 &= \frac{\dot{\alpha}}{4} \left[\frac{\sin(\dot{\alpha} - 2\dot{\beta}) t}{(\dot{\alpha} - 2\dot{\beta})} + \frac{\sin(\dot{\alpha} + 2\dot{\beta}) t}{(\dot{\alpha} + 2\dot{\beta})} \right]_0^T
 \end{aligned}$$

Now, assume that the inner gimbal rate is n times the outer gimbal rate, and that the integration interval (T) is equal to the outer gimbal period of revolution. Then, the integral can be evaluated as



MICROCOPY RESOLUTION TEST CHART
NATIONAL BUREAU OF STANDARDS-1963-A

$$\int_0^T \dot{\alpha} \cos \alpha \sin^2 \beta dt = \frac{1}{2} \sin 2\pi - \frac{1}{4} \left[\frac{\sin(1-2n)2\pi}{(1-2n)} + \frac{\sin(1+2n)2\pi}{(1+2n)} \right]$$

= 0 for all integer N

All except two integrals in Table A-1 reduce to zero over one outer gimbal period, for integer N. The two exceptions are

$$\int_0^T \dot{\alpha} \sin^2 \beta dt \quad \text{and} \quad \int_0^T \dot{\alpha} \cos^2 \beta dt$$

both of which give $\dot{\alpha}T/2$ over the period T. But, by reversing the outer gimbal rate after each successive revolution of 360° , these two give zero net over intervals of $2T$. The periodic reversal of $\dot{\alpha}$ has another benefit as well; it causes every integral that has $\dot{\alpha}$ as a factor to have a mean value of zero (providing that any restriction on the ratio of gimbal rates is observed). The result is that attitude error will tend to be more nearly zero-mean, which in turn produces a lower growth of velocity error through the $\underline{\Psi} \times \underline{a}$ term.

CONDITIONS FOR COMMUTATION OF ACCELEROMETER ERRORS

The velocity error expression is

$$\dot{\delta \underline{V}} = \underline{W} \underline{\dot{e}}_a \tag{A-20}$$

where \underline{e}_a is a vector formed from the accelerometer errors (bias, scale factor, misalignment), and the elements of the matrix W take the general form:

$$w_{ij} = \sum_{k=1}^N b_k g_k(t) \tag{A-21}$$

in which $g_k(t)$ is the k th of N time-dependent functions, and the b_k 's are a function of the components of nongravitational acceleration, \underline{a} .

If all accelerometer errors are taken to be constant over an integration interval T (the period of the outer gimbal motion), and if the components of nongravitational acceleration are also essentially constant over T , Equation A-20 has the solution:

$$\delta \underline{V}(T) = \left[\int_0^T \underline{W}(t) dt \right] \underline{g}_a \quad (A-22)$$

which produces a zero value if:

$$\int_0^T g_k(t) dt = 0 \quad k = 1, 2, \dots, N$$

The integral functions that appear in the solution of the velocity error equations are defined in Table A-2, some of which are the same as those appearing in the attitude error equations. As can be seen from Table A-2, all but eight of the integrals can be made to produce a zero value at the end of each complete revolution of the outer gimbal. However, since none of the integrals associated with accelerometer errors involve the outer gimbal rate, reversal of the outer gimbal motion will not produce a zero value at the end of $2T$. Therefore, the contribution to velocity error represented by these eight terms will be generally monotonic. The accelerometer errors associated with these integrals are scale factor and misalignment errors, and the integrals are associated with error in the vertical direction (i.e., in the direction of the gravity vector). Furthermore, the integrals:

$$\int \sin^2 \alpha \cos \beta dt \quad \int \cos^2 \alpha \cos \beta dt \quad \int \sin 2\alpha \sin \beta dt$$

will not produce a zero value over T if the ratio of inner gimbal to outer gimbal rate (n) is 2. Therefore, an n value of 3 or higher should be used.

TABLE A-2. INTEGRAL FUNCTIONS FOR VELOCITY ERROR PROPAGATION

	$\int g_k(t)dt$	Acceptable Ratio of Gimbal Rates*
Originating from Accelerometer Bias Errors	$\int \sin \alpha dt$	All n
	$\int \cos \alpha dt$	All n
	$\int \sin \theta dt$	All n
	$\int \cos \theta dt$	All n
	$\int \sin \alpha \sin \theta dt$	$n \neq 1$
	$\int \sin \alpha \cos \theta dt$	All n
	$\int \cos \alpha \sin \theta dt$	All n
	$\int \cos \alpha \cos \theta dt$	$n \neq 1$
Originating from Accelerometer Scale Factor and Misalignment Errors	$\int \sin^2 \alpha dt$	All n
	$\int \sin^2 \theta dt$	All n
	$\int \sin^2 \alpha dt$	No n
	$\int \cos^2 \alpha dt$	No n
	$\int \sin^2 \theta dt$	No n
	$\int \cos^2 \theta dt$	No n
	$\int \sin^2 \alpha \sin \theta dt$	All n
	$\int \sin^2 \alpha \cos \theta dt$	$n \neq 2$
	$\int \cos^2 \alpha \sin \theta dt$	All n
	$\int \cos^2 \alpha \cos \theta dt$	$n \neq 2$
	$\int \sin \alpha \sin^2 \theta dt$	All n

* The ratio (n) of inner to outer gimbal rates that produces a zero value of the integral over the period of the outer gimbal motion

TABLE A-2. INTEGRAL FUNCTIONS FOR VELOCITY ERROR PROPAGATION (concluded)

		Acceptable Ratio of Gimbal Rates
Originating from Accelerometer Scale Factor and Misalignment Errors	$\int g_k(t)dt$	
	$\int \cos a \sin^2 b dt$	All n
	$\int \sin a \cos^2 b dt$	All n
	$\int \cos a \cos^2 b dt$	All n
	$\int \sin 2a \sin b dt$	$n \neq 2$
	$\int \sin 2a \cos b dt$	All n
	$\int \sin a \sin 2b dt$	All n
	$\int \cos a \sin 2b dt$	All n
	$\int \sin^2 a \sin^2 b dt$	No n
	$\int \sin^2 a \cos^2 b dt$	No n
	$\int \cos^2 a \sin^2 b dt$	No n
	$\int \cos^2 a \cos^2 b dt$	No n
	$\int \sin^2 a \sin 2b dt$	All n
	$\int \cos^2 a \sin 2b dt$	All n
	$\int \sin 2a \sin^2 b dt$	All n
$\int \sin 2a \cos^2 b dt$	All n	
$\int \sin 2a \sin 2b dt$	$n \neq 1$	

APPENDIX B

NAVIGATION ERROR MODEL

APPENDIX B

NAVIGATION ERROR MODEL

The navigation error equations used as the basis for performance analysis are defined in this appendix, together with a discretization procedure for representing the error model in the form of difference equations.

The navigation error model assumed is a ' Ψ -angle' formulation, which is a classic set of navigation error equations applied to either strapdown or platform systems. The ' Ψ -angle' error model may be expressed in the following form:

$$\dot{\underline{\Psi}} = \underline{\varepsilon}_g - (\underline{\rho} + \underline{\Omega}) \times \underline{\Psi} \tag{B-1}$$

$$\begin{aligned} \dot{\underline{\delta Y}} = \underline{\varepsilon}_a - \underline{\Psi} \times \underline{A}^L - (2\underline{\Omega} + \underline{\rho}) \times \underline{\delta Y} - \omega_s^2 \underline{\delta R} \\ + 3\omega_s^2 (\underline{\delta R} \cdot \underline{R}/R) \underline{R}/R + \underline{\delta a} \end{aligned} \tag{B-2}$$

$$\dot{\underline{\delta R}} = \underline{\delta Y} - \underline{\rho} \times \underline{\delta R} \tag{B-3}$$

where:

- $\underline{\Psi}$ = attitude error vector
- $\underline{\delta Y}$ = velocity error vector
- $\underline{\delta R}$ = position error vector
- $\underline{\rho}$ = angular velocity vector of local vertical reference frame relative to an earth-fixed frame
- $\underline{\Omega}$ = angular velocity vector of the earth relative to an inertial frame
- \underline{A}^L = vehicle nongravitational acceleration
- \underline{R} = radius vector from earth's center to vehicle
- R = magnitude of \underline{R}
- ω_s = Schuler frequency = $\sqrt{g/R}$

$\underline{\epsilon}_g$ = gyro output error vector

$\underline{\epsilon}_a$ = accelerometer output error vector

δg = gravity error

and it is assumed that all vectors are expressed with components in a local-vertical navigational reference frame.

The total gyro and accelerometer error vectors are expressed in terms of individual sensor errors as

$$\underline{\epsilon}_g = CH\underline{X}_g \quad (B-4)$$

$$\underline{\epsilon}_a = G\underline{X}_a \quad (B-5)$$

where:

\underline{X}_g = vector of gyro errors (bias plus random noise)

\underline{X}_a = vector of accelerometer errors (bias plus random noise)

C = transformation matrix relating inertial sensor assembly reference frame to the local-vertical frame

G = coefficient matrix that transforms the collection of accelerometer errors into a net acceleration error in the sensor assembly reference frame

H = coefficient matrix that transforms the collection of gyro errors into a net angular rate error in the sensor assembly reference frame

If the inertial navigator is strapdown, then C is defined to be the direction cosine matrix relating the vehicle body axes to the local-vertical frame. If the inertial navigator is of the platform type, the matrix C is the identity matrix. Thus, Equations B-1 through B-5 are applicable to both types of navigation system, with the appropriate choice for the matrix C. The inertial navigation system error equations given by Equations B-1 through B-5 can be conveniently expressed in the generalized partitioned form:

$$\begin{bmatrix} \dot{\underline{Y}} \\ \dot{\underline{X}} \end{bmatrix} = \begin{bmatrix} F_{11} & F_{12} \\ 0 & F_{22} \end{bmatrix} \begin{bmatrix} \underline{Y} \\ \underline{X} \end{bmatrix} + \begin{bmatrix} G_{11} & 0 \\ 0 & G_{22} \end{bmatrix} \begin{bmatrix} \eta_1 \\ \eta_2 \end{bmatrix} \quad (B-6)$$

where:

\underline{Y} = vector of navigation errors

\underline{X} = vector of sensor errors

It is desirable to discretize Equation B-6 in the partitioned form:

$$\underline{Y}_n = \phi_{11} \underline{Y}_{n-1} + \phi_{12} \underline{X}_{n-1} + \xi_{1n}$$

$$\underline{X}_n = \phi_{22} \underline{X}_{n-1} + \xi_{2n}$$

where:

ξ_1 and ξ_2 are appropriate noise vectors.

The discretization of the sensor states normally presents no problem since it is commonly assumed that sensor errors are adequately represented by either of the following two forms

$$\dot{b} = \eta - \frac{b}{\tau} \quad (\text{first-order Gauss-Markov process})$$

$$\dot{b} = \eta \quad (\text{random walk})$$

where:

- b = sensor bias
- τ = correlation time of process
- η = white noise

If the sensor error is a first-order Gauss-Markov process, the discrete transition and noise variance parameters (Φ, Γ) are given by:

$$\Phi = e^{-t/\tau}$$

$$\Gamma = \sigma^2(1 - e^{-2t/\tau})$$

where σ is the steady-state standard deviation, and τ is the transition time.

When the sensor error follows a random walk type variation, the parameters are

$$\begin{aligned}\Phi &= 1 \\ \Gamma &= Nt\end{aligned}$$

where N is the spectral intensity of the white noise function, η and is expressed in convenient units as

$$N = \left(\frac{\text{standard deviation of change 1 hour}}{60} \right)^2$$

The navigation error transition matrix can be discretized by using a Piccard-type expansion and then solving by numerical integration. The result is given in Tables B-1 and B-2 for a comprehensive set of sensor errors. If, as in this case, the gyro and accelerometer misalignments (non-orthogonalities) are given as constant random errors, only nine misalignment angles need be defined. Either the gyro triad or the accelerometer triad may be designated as

TABLE B-1. SELF-DEPENDENT NAVIGATION STATE TRANSITION MATRIX

	ψ_1	ψ_2	ψ_3	δV_1	δV_2	δV_3	δR_1	δR_2	δR_3
ψ_1	1.0	$\int (\rho_3 + \rho_2) dt$	$-\int (\rho_2 + \rho_1) dt$						
ψ_2	$-\int (\rho_3 + \rho_1) dt$	1.0	$\int (\rho_1 + \rho_2) dt$						
ψ_3	$\int (\rho_2 + \rho_1) dt$	$-\int (\rho_1 + \rho_2) dt$	1.0						
δV_1		$-\int a_3^1 dt$	$\int a_2^1 dt$	$\cos \omega_g t$	$\int (\rho_3 + 2\rho_2) dt$	$-\int (\rho_2 + 2\rho_1) dt$	$-\omega_g \sin \omega_g t$		
δV_2	$\int a_3^1 dt$		$-\int a_2^1 dt$	$-\int (\rho_3 + 2\rho_2) dt$	$\cos \omega_g t$	$\int (\rho_1 + 2\rho_3) dt$	$-\omega_g \sin \omega_g t$		
δV_3	$-\int a_2^1 dt$	$\int a_1^1 dt$		$\int (\rho_2 + 2\rho_1) dt$	$-\int (\rho_1 + 2\rho_3) dt$	$\cosh \sqrt{2} \omega_g t$			$\sqrt{2} \omega_g \sinh \sqrt{2} \omega_g t$
δR_1		$-\int \int a_3^1 dt dt$	$\int \int a_2^1 dt dt$	$\frac{\sin \omega_g t}{\omega_g}$			$\cos \omega_g t$	$\int \rho_3 dt$	
δR_2	$\int \int a_3^1 dt dt$		$-\int \int a_2^1 dt dt$		$\frac{\sin \omega_g t}{\omega_g}$		$-\int \rho_3 dt$	$\cos \omega_g t$	$\int \rho_1 dt$
δR_3	$-\int \int a_2^1 dt dt$	$\int \int a_1^1 dt dt$				$\frac{\sinh \sqrt{2} \omega_g t}{\sqrt{2} \omega_g}$	$\int \rho_2 dt$	$-\int \rho_1 dt$	$\cosh \sqrt{2} \omega_g t$

a_1^1, a_2^1, a_3^1 = nongravitational acceleration components in local vertical frame

ρ_1, ρ_2, ρ_3 = components of earth angular velocity in local vertical frame

ρ_1, ρ_2, ρ_3 = components of local vertical frame rotational velocity due to vehicle translational motion

ω_g = Schuler frequency

TABLE B-2. SENSOR-DRIVEN NAVIGATION STATE TRANSITION MATRIX

	1, 2, 3 Gyro bias	4, 5, 6 Gyro Scale Factor	7, 8, 9 Gyro Misalignment	10, 11, 12 Gyro Sensitivity	13, 14, 15 Gyro "n" Sensitivity	16, 17, 18 Accel Bias	19, 20, 21 Accel Scale Factor	22, 23, 24 Accel Misalignment	25, 26, 27 Accel Nonlinearity
ψ	$G_{11} = \int \omega_1 dt$	$G_{12} = \int \omega_2 dt$	$G_{13} = \int \omega_3 dt$	$G_{14} = \int \omega_4 dt$	$G_{15} = \int \omega_5 dt$				
δV	$G_{21} = \int a_1 dt$	$G_{22} = \int a_2 dt$	$G_{23} = \int a_3 dt$	$G_{24} = \int a_4 dt$	$G_{25} = \int a_5 dt$	$A_{11} = \int \omega_1 dt$	$A_{12} = \int \omega_2 dt$	$A_{13} = \int \omega_3 dt$	$A_{14} = \int \omega_4 dt$
δH	$G_{31} = \int \omega_1 dt$	$G_{32} = \int \omega_2 dt$	$G_{33} = \int \omega_3 dt$	$G_{34} = \int \omega_4 dt$	$G_{35} = \int \omega_5 dt$	$A_{21} = \int \omega_1 dt$	$A_{22} = \int \omega_2 dt$	$A_{23} = \int \omega_3 dt$	$A_{24} = \int \omega_4 dt$

$$G_1 = \begin{bmatrix} \omega_1 & 0 & 0 \\ 0 & \omega_2 & 0 \\ 0 & 0 & \omega_3 \end{bmatrix}$$

$$G_2 = \begin{bmatrix} \omega_2 & 0 & 0 \\ 0 & \omega_3 & 0 \\ 0 & 0 & \omega_4 \end{bmatrix}$$

$$G_3 = \begin{bmatrix} \omega_3 & 0 & 0 \\ 0 & \omega_4 & 0 \\ 0 & 0 & \omega_5 \end{bmatrix}$$

$$A_1 = \begin{bmatrix} a_1 & 0 & 0 \\ 0 & a_2 & 0 \\ 0 & 0 & a_3 \end{bmatrix}$$

$$A_2 = \begin{bmatrix} a_2 & 0 & 0 \\ 0 & a_3 & 0 \\ 0 & 0 & a_4 \end{bmatrix}$$

$$A_3 = \begin{bmatrix} a_3 & 0 & 0 \\ 0 & a_4 & 0 \\ 0 & 0 & a_5 \end{bmatrix}$$

$$A = \begin{bmatrix} 0 & -a_3 & a_2 \\ a_1 & 0 & -a_1 \\ -a_2 & a_1 & 0 \end{bmatrix}$$

$\omega_1, \omega_2, \omega_3$: nominal body angular rates

a_1, a_2, a_3 : nominal body non-gravitational accelerations

a_1, a_2, a_3 : non-gravitational acceleration components in local vertical frame

C : sensor to local vertical transformation matrix

the "reference" triad and assigned three misalignment angles, with six misalignment angles for the remaining triad. In this study, the gyros have six misalignment angles, and the accelerometers have three.

The discretization algorithms in Tables B-1 and B-2 are valid over times that are small compared to the Schuler period and the sensor correlation times. The transition and noise matrixes can be extended over any time by the chain rules:

$$\Phi(t_n, t_0) = \Phi_n \Phi(t_{n-1}, t_0)$$

$$\Gamma(t_n, t_0) = \Phi_n \Gamma(t_{n-1}, t_0) \Phi_n^T + \Gamma_n$$

where:

Φ_n = incremental transition matrix for interval t_{n-1} to t_n

Γ_n = incremental noise covariance matrix for interval t_{n-1} to t_n

The covariance matrix, P , of the error states can be reconstructed at any time from:

$$P_n = \Phi(t_n, t_0) P_0 \Phi^T(t_n, t_0) + \Gamma(t_n, t_0)$$

The error model defined by Equations B-1 through B-5 also applies, with minor modification, to alignment and calibration. The principal difference is that δR is a fixed error and has no variation with time. Also, since the error equations presume small angles, a coarse level and azimuth alignment is implied as a prerequisite for their use.

In addition to the sensor biases, the navigation error equations are driven by two additional sources of random error: 1) sensor random noise, and 2) gravity errors. These additional error sources are accounted for by means of the incremental noise covariance matrix defined in Table B-3. The white noise originating from the gyros, as characterized by the spectral intensity matrix N_g , leads to the attitude random walk. The white noise originating from the accelerometers (absent in the present application) is characterized by the spectral intensity matrix N_a in Table B-3.

TABLE B-3. NAVIGATION STATES NOISE COVARIANCE MATRIX

	ψ	δV	δR
ψ	$q_{11} = \int C N_g C^T dt$	$q_{12} = \int q_{11} A^T dt$	$q_{13} = \int q_{12} dt$
δV	$q_{21} = q_{12}^T$	$q_{22} = \int A q_{12} dt + (\int A q_{12} dt)^T + (N_a + N_v)t$	$q_{23} = \int A q_{13} dt + \int q_{22} dt$
δR	$q_{31} = q_{13}^T$	$q_{32} = q_{23}^T$	$q_{33} = \int q_{23} dt + (\int q_{23} dt)^T$

N_g = Spectral intensity matrix of gyro white noise

N_a = Spectral intensity matrix of accelerometer white noise

N_v = Spectral intensity matrix of white noise originating in local-vertical frame due to gravity errors

C = Sensor to local vertical transformation matrix

$$A = \begin{bmatrix} 0 & -a_3^L & a_2^L \\ a_3^L & 0 & -a_1^L \\ -a_2^L & a_1^L & 0 \end{bmatrix}$$

a_1^L, a_2^L, a_3^L = local-vertical components of nongravitational acceleration

APPENDIX C

SENSOR QUANTIZATION ERROR MODEL

APPENDIX C

SENSOR QUANTIZATION ERROR MODEL

The discrete output of inertial instruments causes an error due to quantization. That is, if the true integral of the sensed rate or acceleration over a given iteration interval is not equal to an integer number of pulses, the fractional pulse will be "saved" and output over the next interval. No fractional pulses are ever lost and the output of the instruments could be accumulated indefinitely, with a maximum error of one pulse. This property provides the basis for mathematically defining quantization error.

Define the quantization error over the n th iteration interval as q_n . Also, define the accumulated quantization error as η_n . Then:

$$\eta_n = \eta_{n-1} + q_n \quad (C-1)$$

The cumulative quantization error, η_n , constitutes a random uncorrelated sequence with uniform distribution. Rearranging Equation C-1, the quantization error over the n th iteration interval is expressed as

$$q_n = \eta_n - \eta_{n-1} \quad (C-2)$$

Thus, quantization error is characterized as the difference between two successive members of a random independent set.

ATTITUDE ERROR DUE TO GYRO QUANTIZATION

Consider attitude error in a rotational environment with the gyros skewed. The attitude matrix differential equation for this case is

$$\dot{C} = C (A\omega) \quad (C-3)$$

where:

C = orthogonal direction cosine matrix

A = transformation matrix from skewed sensor axes to a set of orthogonal sensor reference axes

ω = angular rate measured by gyros

and $\{\underline{y}\}$ denotes a skew-symmetric matrix formed from the components of a vector \underline{y} .

The discrete algorithm for updating Equation C-3 is

$$C_n = C_{n-1} \left[I + \{A\theta\} + \frac{1}{2}\{A\theta\}^2 + \dots \right] \quad (C-4)$$

where:

$$\theta = \int_{t_{n-1}}^{t_n} \omega dt \quad (C-5)$$

Directly from Equation C-4, the error in C is

$$\begin{aligned} \delta C_n = & \delta C_{n-1} \left[I + \{A\theta\} + \frac{1}{2}\{A\theta\}^2 + \dots \right] \\ & + C_{n-1} \left[\{A\delta\theta\} + \frac{1}{2}\{A\delta\theta\} \{A\theta\} + \frac{1}{2}\{A\theta\} \{A\delta\theta\} + \dots \right] \end{aligned} \quad (C-6)$$

where $\delta\theta$ is the error in the incremental gyro output defined by Equation C-5.

Since gyro quantization error can only cause a rotational error, the erroneous C matrix can be expressed as

$$\hat{C}_n = \left[I - \{\Psi_n\} \right] C_n \quad (C-7)$$

where:

$\underline{\Psi}$ = misalignment angle vector
 \hat{C} = erroneous C Matrix

From Equation C-7, the error in C can be expressed as

$$\delta C_n = -\{\underline{\Psi}_n\} C_n \quad (C-8)$$

Substituting Equations C-8 and C-4 into C-6 results in:

$$\begin{aligned} \{\underline{\Psi}_n\} C_n = & \{\underline{\Psi}_{n-1}\} C_{n-1} \left[I + \{A\theta\} + \frac{1}{2}\{A\theta\}^2 + \dots \right] \\ & - C_n \left[I - \{A\theta\} + \frac{1}{2}\{A\theta\}^2 + \dots \right] \left[\{A\delta\theta\} + \frac{1}{2}\{A\delta\theta\} \{A\theta\} + \frac{1}{2}\{A\theta\} \{A\delta\theta\} + \dots \right] \end{aligned} \quad (C-9)$$

Using the identity:

$$\{a\}\{b\} - \{b\}\{a\} = \{a \times b\} = \{a\}\{b\}$$

and neglecting higher-order terms, Equation C-9 reduces to:

$$\{\underline{\Psi}_n\} = \{\underline{\Psi}_{n-1}\} - C_n \left[\{A\delta\theta\} - 1/2 \{A\theta\} \{A\delta\theta\} \right] C_n^T \quad (C-10)$$

which, in vector form, is expressed as

$$\underline{\Psi}_n = \underline{\Psi}_{n-1} - \bar{C}_n A \delta \theta \quad (C-11)$$

where \bar{C}_n is defined as

$$\bar{C}_n = C_n \left[I - 1/2 \{A\theta\} \right]$$

and may be taken to be the true value of C at the midpoint of the interval.

Equation C-11 defines a generalized recursive relationship for attitude error propagation which, when $\delta\Theta$ represents gyro quantization error, takes the specific form:

$$\underline{\Psi}_n = \underline{\Psi}_{n-1} - \bar{C}_n \Lambda (\underline{n}_n - \underline{n}_{n-1}) \quad (C-12)$$

Equation (C-12) can be expanded as

$$\begin{aligned} \underline{\Psi}_n &= C_1 \Lambda \underline{n}_1 \\ &+ C_2 \Lambda \underline{n}_2 - [(\bar{C}_2 - \bar{C}_1) + \bar{C}_1] \Lambda \underline{n}_1 \\ &+ \bar{C}_3 \Lambda \underline{n}_3 - [(\bar{C}_3 - \bar{C}_2) + \bar{C}_2] \Lambda \underline{n}_2 \\ &+ \dots \\ &+ \bar{C}_n \Lambda \underline{n}_n - [(\bar{C}_n - \bar{C}_{n-1}) + \bar{C}_{n-1}] \Lambda \underline{n}_{n-1} \end{aligned}$$

which, after cancellations, reduces to:

$$\underline{\Psi}_n = \bar{C}_n \Lambda \underline{n}_n - \sum_{i=1}^{n-1} \Delta C_{i-1} \Lambda \underline{n}_{i-1} \quad (C-13)$$

where:

$$\Delta C_{i-1} = \bar{C}_i - C_{i-1}$$

The covariance of $\underline{\Psi}$ is determined directly from Equation C-13 as

$$E(\underline{\Psi}_n \underline{\Psi}_n^T) = \bar{C}_n \Lambda \Lambda^T \bar{C}_n^T \sigma_g^2 + \sum_{i=1}^{n-1} \Delta C_i \Lambda \Lambda^T \Delta C_i^T \sigma_g^2 \quad (C-14)$$

where:

$$\sigma_g^2 = E(\underline{n} \underline{n}^T)$$

Equation C-14 indicates that gyro quantization produces a bounded attitude error (first term), plus an unbounded error component (second term). The unbounded component will grow at a rate proportional to the rotational velocity of the gyro triad.

Another form for expressing attitude error growth, which is more convenient for covariance analysis, is given by the equation set:

$$\begin{aligned}\underline{\psi}_n &= \bar{C}_n \underline{A}_n + \underline{u}_{n-1} \\ \underline{u}_n &= \underline{u}_{n-1} - \Delta C_n \underline{A}_n\end{aligned}\tag{C-15}$$

which is simply a rearrangement of Equation C-13 with the summation expressed recursively.

VELOCITY ERROR DUE TO GYRO AND ACCELEROMETER QUANTIZATION

The computed direction cosine matrix, C , is used to transform accelerations measured in the accelerometer axes into components in the reference frame:

$$\dot{\underline{v}} = C \underline{a}\tag{C-16}$$

where:

- \underline{v} = velocity in reference frame
- \underline{a} = measured acceleration in sensor frame,

It is assumed that the accelerometers form an orthogonal triad that coincides with the orthogonal gyro reference axes.

A discrete algorithm for updating Equation C-16 is

$$\underline{V}_n = \underline{V}_{n-1} + \bar{C}_n \underline{v}_n \quad (C-17)$$

where \underline{v}_n is the incremental accelerometer output, and \bar{C} is the direction cosine matrix at the midpoint of the computational interval. The error incurred in accumulating velocity is

$$\begin{aligned} \delta \underline{V}_n &= \delta \underline{V}_{n-1} + \delta \bar{C}_n \underline{v}_n + \bar{C}_n \delta \underline{v}_n \\ &= \delta \underline{V}_{n-1} - \{\bar{\Psi}_n\} \bar{C}_n \underline{v}_n + \bar{C}_n \delta \underline{v}_n \\ &= \delta \underline{V}_{n-1} - \bar{\Psi}_n \times \underline{v}_n^r + \bar{C}_n \delta \underline{v}_n \\ &= \delta \underline{V}_{n-1} + \{\underline{v}_n^r\} \bar{\Psi}_n + \bar{C}_n \delta \underline{v}_n \end{aligned} \quad (C-18)$$

where:

$$\underline{v}_n^r = \bar{C}_n \underline{v}_n$$

and where the misalignment vector $\bar{\Psi}$ is defined as

$$\bar{\Psi}_n = 1/2(\bar{\Psi}_n + \bar{\Psi}_{n-1})$$

which, for all practical purposes, is accurately approximated by $\bar{\Psi}_n = \bar{\Psi}_{n-1}$.

Equation C-18 can be decomposed into two parts (to separate the contributions due to gyro and accelerometer quantization errors) as follows.

$$\delta \underline{V}_n^a = \delta \underline{V}_{n-1}^a + \bar{C}_n \delta \underline{v}_n \quad (C-19)$$

$$\delta \underline{V}_n^g = \delta \underline{V}_{n-1}^g + \{\underline{v}_n^r\} \bar{\Psi}_n \quad (C-20)$$

Thus, the effect of accelerometer quantization on velocity error has exactly the same form as the effect of gyro quantization error on attitude error. The only difference is that, because the gyros are taken to be skewed, the attitude error equation involves the transformation matrix A. By omitting A and making the substitution ($\delta \underline{v}^a \rightarrow \underline{\psi}$) Equations C-13, C-14, and C-15 are immediately applicable to accelerometer quantization error propagation.

The complete model of gyro and accelerometer quantization effects is summarized in Figure C-1. The model is recursive and operates at the attitude and velocity update frequency.

COVARIANCE ANALYSIS MODEL FOR PROPAGATION OF QUANTIZATION ERRORS

For covariance analysis, we need to express the effect of sensor quantization error over periods of time much longer than the iteration interval of the update equations. The covariance matrix can be determined by solving the discrete covariance equation

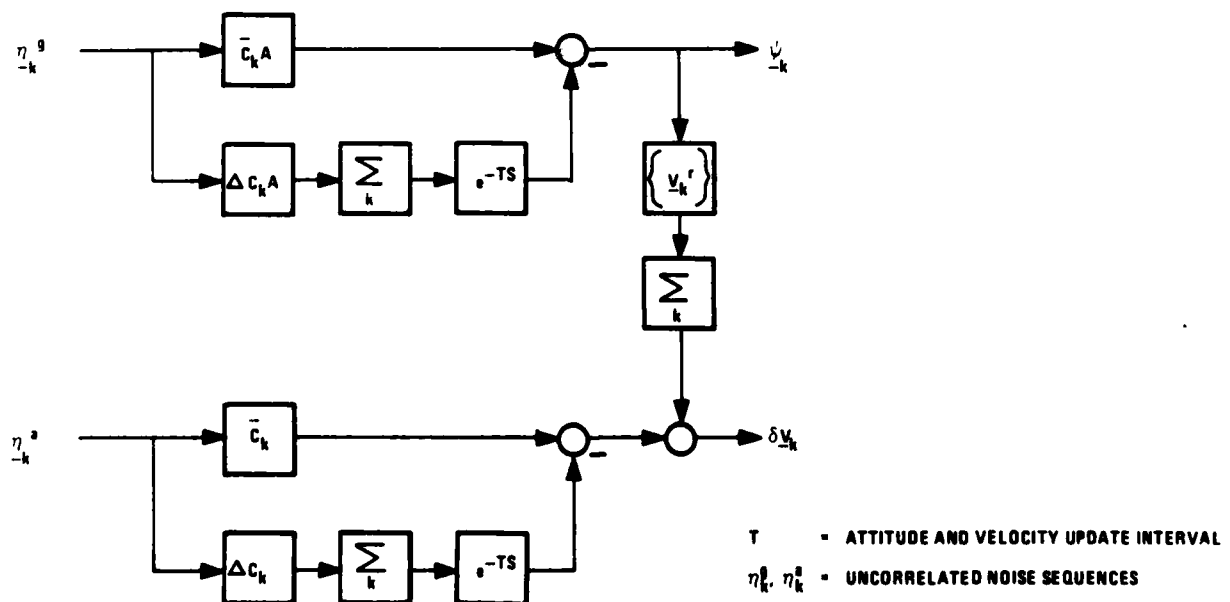


Figure C-1. Deterministic Model of Quantization-Induced Error

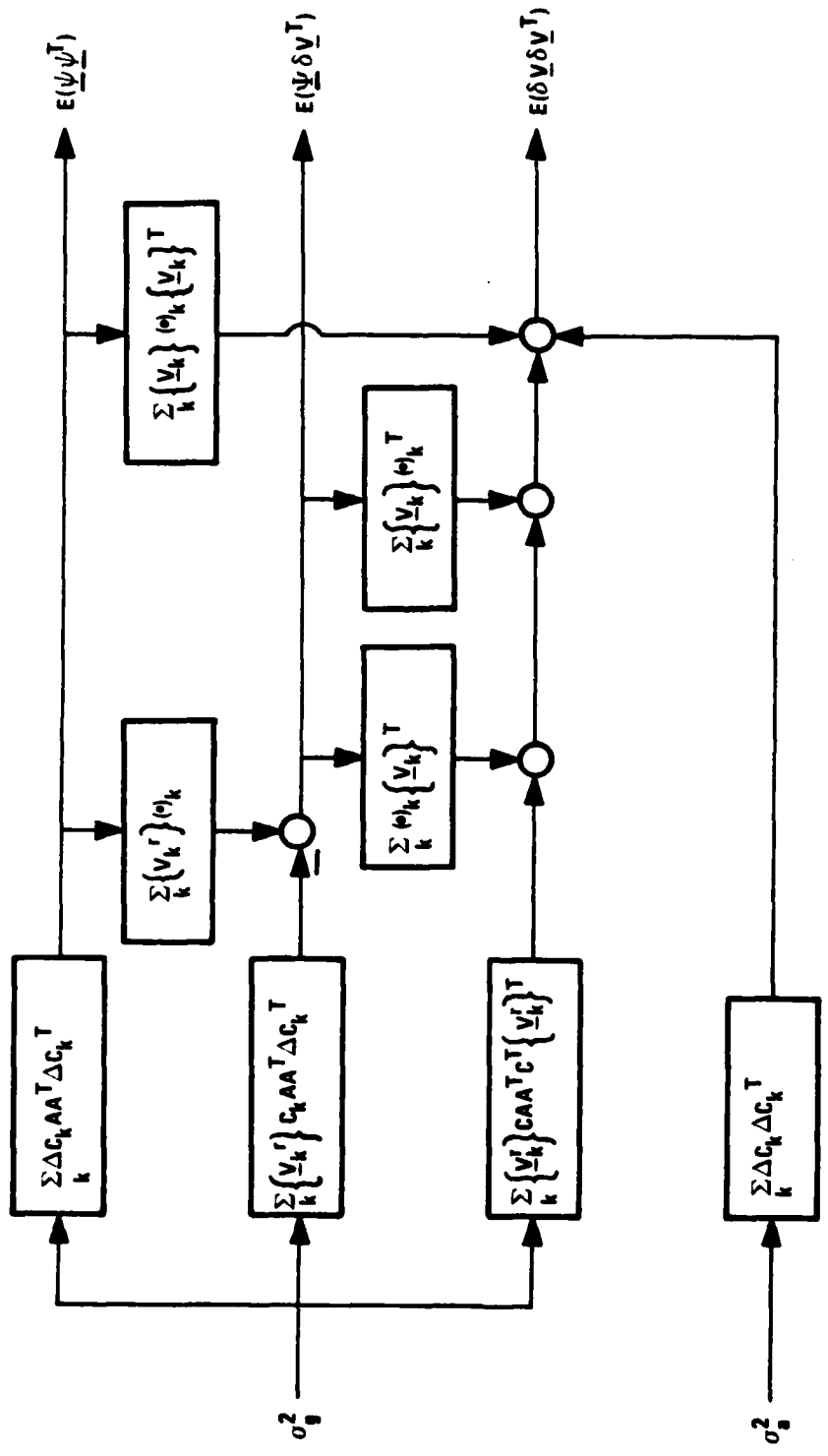
$$P_n = \Phi_n P_{n-1} \Phi_n^T + Q_n \quad (C-21)$$

for the error model defined by Figure C-1. The evaluation of Equation C-21 is straightforward and results in the solution given in Figure C-2. For convenience, the summations can be replaced by continuous integrations, assuming that the variations in \underline{y}^T are relatively smooth. Then, we can write:

$$\begin{aligned} \sum_{k=1}^{n-1} \Delta C_k A A^T \Delta C_k^T &= T \int_0^{t-T} C A A^T C^T dt \\ &= T \int_0^{t-T} C(A_{\Delta t}) A A^T (A_{\Delta t})^T C^T dt \end{aligned}$$

where T is the update interval.

The covariance solution given by Figure C-2 defines the variances and cross covariances of the errors due to sensor quantization over any length of time. In practice, the solution is carried out only over periods of time equal to the discretization interval of the error equations. The noise covariance matrices $E(\underline{\Psi} \underline{\Psi}^T)$, $E(\underline{\Psi} \delta \underline{V}^T)$, and $E(\delta \underline{V} \delta \underline{V}^T)$ then provide the statistical description of a discrete uncorrelated input to the navigation error equations over the interval. After each successive discretization interval, the solution inherent in Figure C-2 is started anew.



$$\sigma_g^2 = \text{VARIANCE OF GYRO QUANTIZATION ERROR} = p_g^2/12$$

$$\sigma_a^2 = \text{VARIANCE OF ACCELEROMETER QUANTIZATION ERROR} = p_a^2/12$$

Figure C-2. Covariance Model for Quantization-Induced Error

END

FILMED

4-85

DTIC